

Condensed Matter Physics with Cold Polar Molecules

G. Pupillo^{1,2}, A. Micheli^{1,2}, H.P. Büchler³, and P. Zoller^{1,2}

¹*Institute for Theoretical Physics, University of Innsbruck, 6020 Innsbruck, Austria*

²*Institute for Quantum Optics and Quantum Information, 6020 Innsbruck, Austria and*

³*Institute for Theoretical Physics III, University of Stuttgart, Pfaffenwaldring 57, 70550 Stuttgart, Germany*

(Dated: November 18, 2018)

I. INTRODUCTION

The realization of Bose Einstein condensates and quantum degenerate Fermi gases with cold atoms has been one of the highlights of experimental atomic physics during the last decade¹, and in view of recent progress in preparing cold molecules we expect a similarly spectacular development for molecular ensembles^{2,3,4,5,6,7,8,9,10,11,12,13,14,15,16,17,18,19,20,21,22,23}.

The outstanding features of the physics of cold atomic and molecular gases are the microscopic knowledge of the many-body Hamiltonians, as realized in the experiments, combined with the possibility to control and tune system parameters via external fields. Examples are the trapping of atoms and molecules with magnetic, electric and optical traps, allowing for the formation of quantum gases in 1D, 2D and 3D geometries, and the tuning of *contact* inter-particle interactions by varying the scattering length via Feshbach resonances^{24,25}. This control is the key for the experimental realization of fundamental quantum phases, as illustrated by the BEC-BCS crossover in atomic Fermi gases^{26,27,28,29,30}, the Kosterlitz-Thouless transition³¹ and the superfluid-Mott insulator quantum phase transition with cold bosonic atoms in an optical lattice^{32,33}. A recent highlight has been the realization of a degenerate magnetic dipolar gas of ⁵²Cr atoms^{34,35,36}. Below we will be mainly interested in heteronuclear molecules prepared in their electronic and vibrational ground state. The new feature of polar molecules is their *large electric dipole moments* associated with rotational excitations. The new aspects in a condensed matter theory of cold polar molecules are the *large dipole-dipole interactions* between molecules. This points towards the possibility of manipulating these strong and long-range interactions with external DC and AC microwave fields. In particular, this raises interesting questions of cold ensembles of polar molecules as *strongly correlated systems*^{37,38,39,40,41,42,43,44,45,46,47,48,49,50,51,52,53,54,55,56,57,58,59}.

Magnetic or electric dipole moments in external fields can give rise to anisotropic, long-range dipole-dipole interactions. Analogous to the case of cold atoms with contact interactions, a key element for the realization of interesting quantum phases and phase transitions with interacting dipolar gases is the capability of controlling and tuning system parameters using external fields. Much work has been recently devoted to the study of cold collisions in dipolar gases^{60,61,62,63,64,65,66}, which in this book is reviewed in the chapters contributed by Hut-

son, Bohn, and Dalgarno. In the context of degenerate molecular gases a significant body of recent work has focused on the regime of *weak interactions*, where the isotropic contact interaction potential competes with the anisotropic long range dipole-dipole interaction. For example, the existence of rotons in weakly-interacting dipolar gases has been predicted^{67,68,69,70,71,72,73,74,75}, while exciting prospects have been envisioned for rotating systems^{76,77,78,79,80,81} and polar molecules in optical lattices^{82,83,84,85,86,87,88,89}. Below we will be mainly interested in the many-body dynamics of polar molecules in the *strongly interacting limit*. In particular, we will discuss a toolbox for engineering interesting many-body Hamiltonians based on the manipulation of the electric dipole moments with external DC and AC fields, and thus of the molecular interactions. This forms the basis for the realization of novel quantum phases in these systems. Our emphasis will be on condensed matter aspects, while we refer to the contribution by Yelin, DeMille and Cote in the present book for application in the context of quantum information processing.

This review is organized as follows. In Sect. II we give a qualitative tour through some of the key ideas of engineering Hamiltonians and of the associated quantum phases. This is followed by two slightly more technical sections, Sect. III A and Sect. III B, where we provide some details of the realization of a 2D setup where particles interact via purely repulsive $1/r^3$ potentials, and where we sketch how to design more complicated interactions by using a combination of AC and DC fields. Finally, Sect. IV deals with the applications of the engineering of interaction potentials in the context of the realization of strongly correlated phases and quantum simulations.

II. OVERVIEW: STRONGLY INTERACTING SYSTEMS OF COLD POLAR MOLECULES

In this section we give a qualitative overview of many-body physics of cold polar molecules with emphasis on strongly interacting systems. In the following sections we will return to the various topics in a more in-depth discussion.

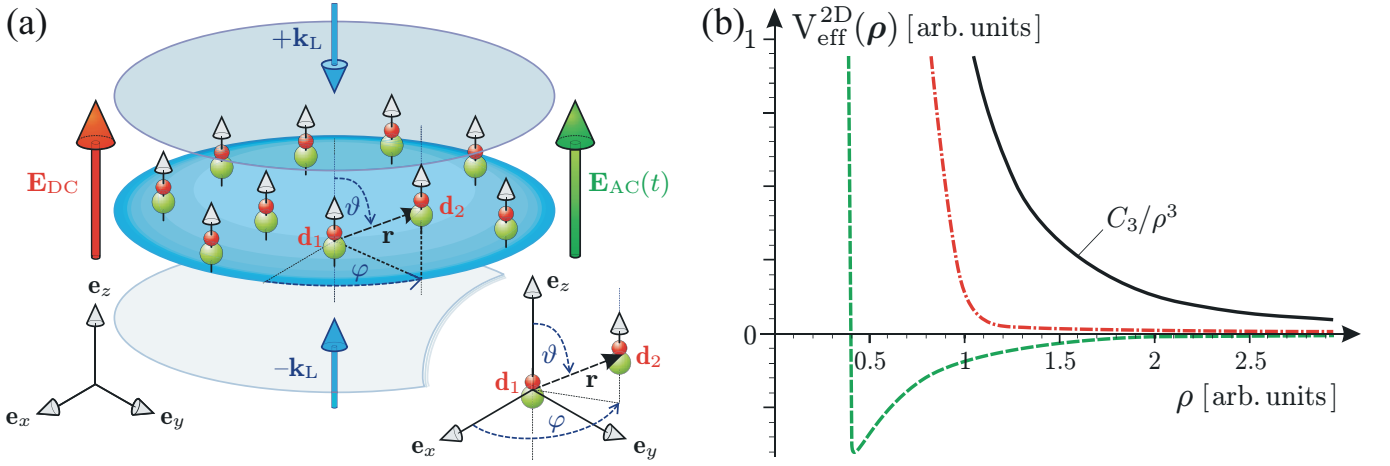


FIG. 1: (a) System setup: Polar molecules are trapped in the (x, y) -plane by an optical lattice made of two counter-propagating laser beams with wavevectors $\pm \mathbf{k}_L = \pm k_L \mathbf{e}_z$, (blue arrows). The dipoles are aligned in the z -direction by a DC electric field $\mathbf{E}_{DC} \equiv E_{DC} \mathbf{e}_z$ (red arrow). An AC microwave field is indicated (green arrow). Inset: Definition of polar (ϑ) and azimuthal (φ) angles for the relative orientation of the inter-molecular collision axis \mathbf{r}_{12} with respect to a space-fixed frame, with axis along z . (b) Qualitative sketch of effective 2D potentials $V_{\text{eff}}^{2D}(\rho)$ for polar molecules confined in a 2D (pancake) geometry. Here, $\rho = r_{12} \sin \vartheta (\cos \varphi, \sin \varphi, 0)$ is the 2D coordinate in the plane $z = 0$ and $\rho = r_{12} \sin \vartheta$ (see Fig. 1, inset). Solid line: Repulsive dipolar potential $V_{\text{eff}}^{2D}(\rho) = D/\rho^3$ induced by a DC electric field. Dash-dotted line: “Step-like” potential induced by a single AC microwave field and a weak DC field. Dashed line: Attractive potential induced by the combination of several AC fields and a weak DC field. The potentials $V_{\text{eff}}^{2D}(\rho)$ and the separation ρ are given in arbitrary units.

A. Effective many body Hamiltonians

Hamiltonians underlying condensed matter physics of N structureless bosonic or fermionic particles have the generic form

$$H_{\text{eff}} = \sum_{i=1}^N \left[\frac{\mathbf{p}_i^2}{2m} + V_{\text{trap}}(\mathbf{r}_i) \right] + V_{\text{eff}}^{3D}(\{\mathbf{r}_i\}), \quad (1)$$

where $\mathbf{p}_i^2/2m$ is the kinetic energy term, and $V_{\text{trap}}(\mathbf{r}_i)$ is a confining potential for the particles. The term $V_{\text{eff}}^{3D}(\{\mathbf{r}_i\})$ represents an effective N -body interaction, which can be expanded as a sum of two-body, three-body interactions *etc.*,

$$V_{\text{eff}}^{3D}(\{\mathbf{r}_i\}) = \sum_{i<j}^N V^{3D}(\mathbf{r}_i - \mathbf{r}_j) + \sum_{i<j<k}^N W^{3D}(\mathbf{r}_i, \mathbf{r}_j, \mathbf{r}_k) + \dots, \quad (2)$$

where in most cases only two-body interactions are considered. Typically, $V_{\text{eff}}^{3D}(\{\mathbf{r}_i\})$ must be interpreted as *effective* interactions valid in a *low energy theory*, obtained by integrating out the high energy degrees of freedom of the system. In the following we will discuss the derivation of such many body Hamiltonians for a cold ensemble of polar molecules in the electronic and vibrational ground state, and show how the effective interactions in these systems can be “designed” on an N -body level via control of rotational excitations with external fields, in a form which is unique to polar molecules.

Our starting point is the Hamiltonian for a gas of cold heteronuclear molecules prepared in their electronic and vibrational ground-state,

$$H(t) = \sum_i^N \left[\frac{\mathbf{p}_i^2}{2m} + V_{\text{trap}}(\mathbf{r}_i) + H_{\text{in}}^{(i)} - \mathbf{d}_i \mathbf{E}(t) \right] + \sum_{i<j}^N V_{\text{dd}}(\mathbf{r}_i - \mathbf{r}_j). \quad (3)$$

Here the first term in the single particle Hamiltonian corresponds to the kinetic energies of the molecules, while $V_{\text{trap}}(\mathbf{r}_i)$ represents a possible trapping potential, as provided, for example, by an optical lattice, or an electric or magnetic traps. The term $H_{\text{in}}^{(i)}$ describes the internal low energy excitations of the molecule, which for a molecule with a closed electronic shell $^1\Sigma(\nu = 0)$ (e.g. of the type SrO, RbCs or LiCs), correspond to the rotational degree of freedom of the molecular axis. This term is well described by a rigid rotor $H_{\text{in}}^{(i)} \equiv H_{\text{rot}}^{(i)} = B \mathbf{J}_i^2$ with B the rotational constant (in the few to tens of GHz regime) and \mathbf{J}_i the dimensionless angular momentum. The rotational eigenstates $|J, M\rangle$ for a quantization axis z , and with eigenenergies $B J(J+1)$ can be coupled by a static (DC) or microwave (AC) field \mathbf{E} via the *electric* dipole moment \mathbf{d}_i , which is typically of the order of a few Debye. For distances outside of the molecular core, the two-body interaction as given by the second line of Eq. (3) is the dipole-dipole interaction

$$V_{\text{dd}}(\mathbf{r}) = \frac{\mathbf{d}_i \cdot \mathbf{d}_j - 3(\mathbf{d}_i \cdot \mathbf{e}_r)(\mathbf{e}_r \cdot \mathbf{d}_j)}{r^3}. \quad (4)$$

Here $r \equiv |\mathbf{r}| = |\mathbf{r}_i - \mathbf{r}_j|$ denotes the distance between two polar molecules, with \mathbf{e}_r the unit vector along the collision axis. In view of the large electric dipole moments this term provides a comparatively strong, long-range anisotropic interaction between the molecules.

The many body dynamics of cold polar molecules is thus governed by an interplay between dressing and manipulating the rotational states with DC and AC fields, and strong dipole-dipole interactions. In the absence of electric fields, the molecules prepared in a ground rotational state $J = 0$ have no net dipole moment, and interact via a van-der-Waals attraction $V_{\text{vdW}} \sim -C_6/r^6$, reminiscent of the interactions of cold Alkali atoms in their electronic ground-states. Electric fields admix excited rotational states and induce static or oscillating dipoles, which will interact via strong dipole-dipole interactions V_{dd} with the characteristic $1/r^3$ dependence of Eq. (4). Note that two parallel dipoles repel each other, while dipoles aligned along the collision axis will attract each other, possibly inducing instabilities in a many-body system. Thus to obtain stable many-particle phases is often possible only in reduced geometries, i.e. in combination with an external trapping potential $V_{\text{trap}}(\mathbf{r}_i)$. Finally, we emphasize that microwave excited rotational states of polar molecules are long-lived, which makes these states available without the penalty of introducing significant decoherence. This is in contrast to atomic systems, where spontaneous emission from laser excited electronic states is one of the main contributions to decoherence.

The connection between the full molecular N -particle Hamiltonian (3) including rotational excitations and dressing fields, and the effective Hamiltonian (1) can be made in a Born-Oppenheimer approximation. If we diagonalize for frozen spatial positions $\{\mathbf{r}_i\}$ of the N molecules the Hamiltonian⁹⁰ $H_{BO} = \sum_i^N [H_{\text{in}}^{(i)} - \mathbf{d}_i \mathbf{E}] + \sum_{i < j}^N V_{dd}(\mathbf{r}_i - \mathbf{r}_j)$, we obtain a set of energy eigenvalues $V_{\text{eff}}^{3D}(\{\mathbf{r}_i\})$, which are interpreted as the effective N -particle potential in the single channel many-body Hamiltonian (1). The dependence of $V_{\text{eff}}^{3D}(\{\mathbf{r}_i\})$ on the electric fields \mathbf{E} provides the basis of the engineering of the many body interactions of two-body, three-body terms *etc.* in (2). The validity of this adiabatic approximation and of the associated decoupling of the Born-Oppenheimer channels will be discussed below.

The above considerations set the stage for a discussion of engineering many-body Hamiltonians for polar molecules, and associated quantum phases. In the following subsections we will discuss specific examples of DC and AC field configurations for designing two-body and three-body interactions, which will be the content of Sects. IIB and IIC below. Our discussion can also be adapted to optical lattices, and thus to a derivation of Hubbard models for polar molecules (Sect. IID). Furthermore, we can extend these derivations to molecules with internal degrees of freedom representing a spin (Sect. IIE). Extended Hubbard models with couplings to phonons are presented in Sect. IIF for molecules trapped

in self-assembled dipolar crystals.

B. Self-assembled crystals.

The conceptually simplest example, although remarkably rich from a physics point of view, is a system of cold polar molecules in a DC electric field under conditions of strong transverse confinement. The setup is illustrated in Fig. 1(a). A weak DC field along the z -direction induces a dipole moment d in the ground state of each molecule. These groundstate molecules interact via the effective dipole-dipole interaction $V_{\text{eff}}^{3D}(\mathbf{r}) = D(r^2 - 3z^2)/r^5$ according to their induced dipoles, with $D = d^2$. For molecules confined to the x, y -plane perpendicular to the electric field this interaction is purely repulsive. For molecules displaced by $z > r/\sqrt{3}$ the interaction becomes attractive, indicating an instability in the many body system. This instability is suppressed by a sufficiently strong 2D confinement with potential a $V_{\text{trap}}(z_i)$ along z , due to, for example, an optical potential induced by an off-resonant light field⁵⁰.

The 2D dynamics in this pancake configuration is described by the Hamiltonian

$$H_{\text{eff}}^{2D} = \sum_i \frac{\mathbf{p}_{\rho i}^2}{2m} + \sum_{i < j} V_{\text{eff}}^{2D}(\rho_{ij}), \quad (5)$$

which is obtained by integrating out the fast z -motion. Equation (5) is the sum of the 2D kinetic energy in the x, y -plane and a repulsive 2D dipolar interaction

$$V_{\text{eff}}^{2D}(\rho) = D/\rho^3, \quad (6)$$

with $\rho_{ij} \equiv (x_j - x_i, y_j - y_i)$ a vector in the x, y -plane [solid line in Fig. 1(b)]. The distinguishing feature of the system described by the Hamiltonian (5) is that tuning the induced dipole moment d drives the system from a weakly interacting gas (a 2D superfluid in the case of bosons), to a crystalline phase in the limit of strong repulsive dipole-dipole interactions. This transition and the crystalline phase have no analog in the familiar atomic Bose gases with short range interactions modelled by a pseudopotential of a given scattering length.

A crystalline phase corresponds to the limit of strong repulsion where particles undergo small oscillations around their equilibrium positions, which is a result of the balance between the repulsive long-range dipole-dipole forces and an additional (weak) confining potential in the x, y -plane. The relevant parameter is

$$r_d \equiv \frac{E_{\text{pot}}}{E_{\text{kin}}} = \frac{D/a^3}{\hbar^2/ma^2} = \frac{Dm}{\hbar^2 a}, \quad (7)$$

which is the ratio of the the interaction energy and the kinetic energy at the mean interparticle distance a . This parameter is tunable as a function of d from r_d small to large. A crystal will form for $r_d \gg 1$, when interactions dominate. For a dipolar crystal, this is the

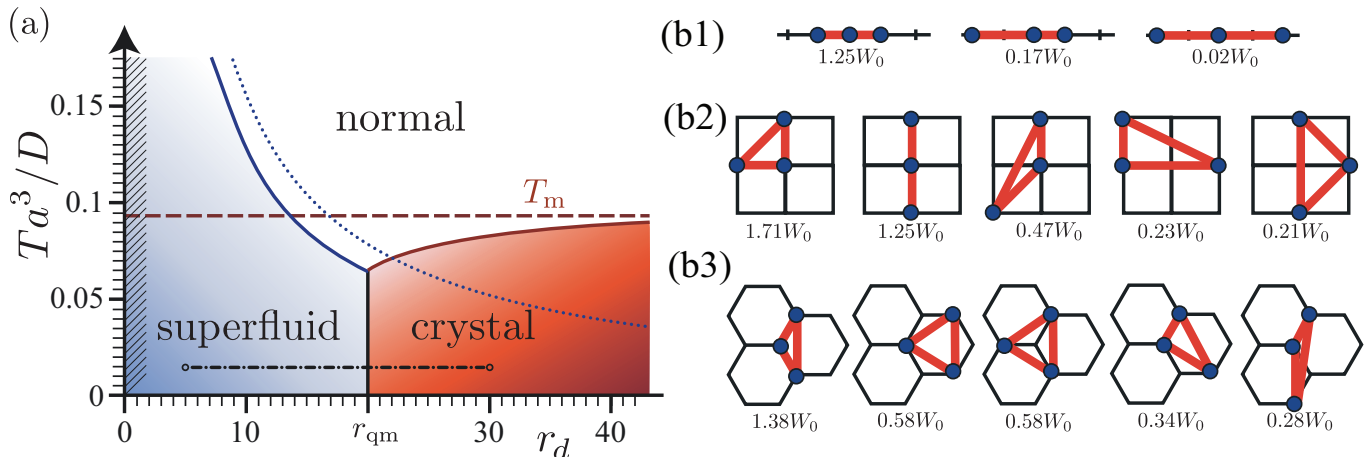


FIG. 2: (a) Tentative phase diagram in the $T - r_d$ plane: crystalline phase for interactions $r_d > r_{QM}$ and temperatures below the classical melting temperature T_m (dashed line). The superfluid phase appears below the upper bound $T < \pi\hbar^2 n/2m$ (dotted line). The quantum melting transition is studied at fixed temperature $T = 0.014D/a^3$ with interactions $r_d = 5 - 30$ (dash-dotted line). The crossover to the unstable regime for small repulsion and finite confinement ω_\perp is indicated (hatched region). (b) Strengths of the dominant three-body interactions W_{ijk} appearing in the Hubbard model of Eq. (9) for different lattice geometries: (b1) one-dimensional setup; (b2) two-dimensional square lattice; (b3) two-dimensional honeycomb lattice. The characteristic energy scale $W_0 = \gamma_2 DR_0^6/a^6$ is discussed following Eq. (41).

limit of large densities, where typically collisions become harmful. However the crystalline phase will protect a cold ensemble of polar molecules from (harmful) close-encounter collisions. This density dependence is in contrast to Wigner crystals with $1/r$ -Coulomb interactions, as realized e.g. with laser cooled trapped ions⁹¹. In this case $r_c = (e^2/a)/\hbar^2/ma^2 \sim a$ and the crystal forms at low densities. In addition, the charge e is a fixed quantity, while d can be varied as a function of the DC field.

Fig. 2(a) shows a tentative phase diagram for a dipolar gas of bosonic molecules in 2D as a function of r_d and temperature T . In the limit of weak interactions $r_d < 1$, the ground state is a superfluid (SF) representing a finite (quasi-)condensate. In the opposite limit of strong interactions $r_d \gg 1$ the polar molecules are in a crystalline phase for temperatures $T < T_m$ with $T_m \approx 0.09D/a^3$, see Ref.⁹⁴. The configuration with minimal energy is a triangular lattice with excitations given by acoustic phonons. In Ref.⁵⁰ we investigated the intermediate strongly interacting regime with $r_d \gtrsim 1$, using a recently developed Path-Integral Monte-Carlo technique (PIMC)⁹⁵, and we determined the critical interaction strength r_{QM} for the quantum melting transition from the crystal into the superfluid. We found the latter to occur at $r_{QM} = 18 \pm 4$, a result which has been confirmed with a number of quantum Monte-Carlo techniques (author?)^{51, 52}.

In Sect. IV below we return to a more detailed discussion of these quantum phases, and in particular of the crystalline phase, and we show that the relevant parameter regime where these phases occur is accessible with polar molecules. Besides the fundamental interest in dipolar quantum gases, the crystalline phase has interesting applications, e.g. in the context of quantum

information⁵⁵. We will return to self-assembled dipolar lattices below in a discussion of Hubbard models.

C. Blue-shielding and three-body interactions

By combining DC and AC fields to dress the manifold of rotational excitations we can design effective interaction potentials $V^{3D}(\mathbf{r}_i - \mathbf{r}_j)$ with (essentially) any given shape as a function of distance. For example, the addition of a single linearly-polarized AC field to the configuration of Fig. 1(a) leads to the realization of the 2D “step-like” potential of Fig. 1(b), where the character of the repulsive potential varies considerably in a small region of space. The derivation of this effective 2D interaction is sketched in Fig. 3 and it is discussed in more detail in Sect. III B 2 below^{50, 66}. The (weak) DC-field splits the first-excited rotational ($J = 1$)-manifold of each molecule by an amount $\hbar\delta$, while a linearly polarized AC-field with Rabi frequency Ω is blue-detuned from the ($|g\rangle - |e\rangle$)-transition by $\hbar\Delta$, see Fig. 3(a). Because of $\hbar\delta$ and the choice of polarization, for distances $\rho \gg (d^2/\hbar\delta)^{1/3}$ the relevant single-particle states for the two-body interaction reduce to the states $|g\rangle$ and $|e\rangle$ of each molecule. Figure 3(b) shows that the dipole-dipole interaction splits the excited state manifold of the two-body rotational spectrum, making the detuning Δ *position-dependent*. As a consequence, the combined energies of the bare groundstate of the two-particle spectrum and of a microwave photon become degenerate to the energy of a (symmetric) excited state at a characteristic resonant (Condon) point $\rho_C = (d^2/\hbar\Delta)^{1/3}$, which is represented by an arrow in Fig. 3(b). At this Con-

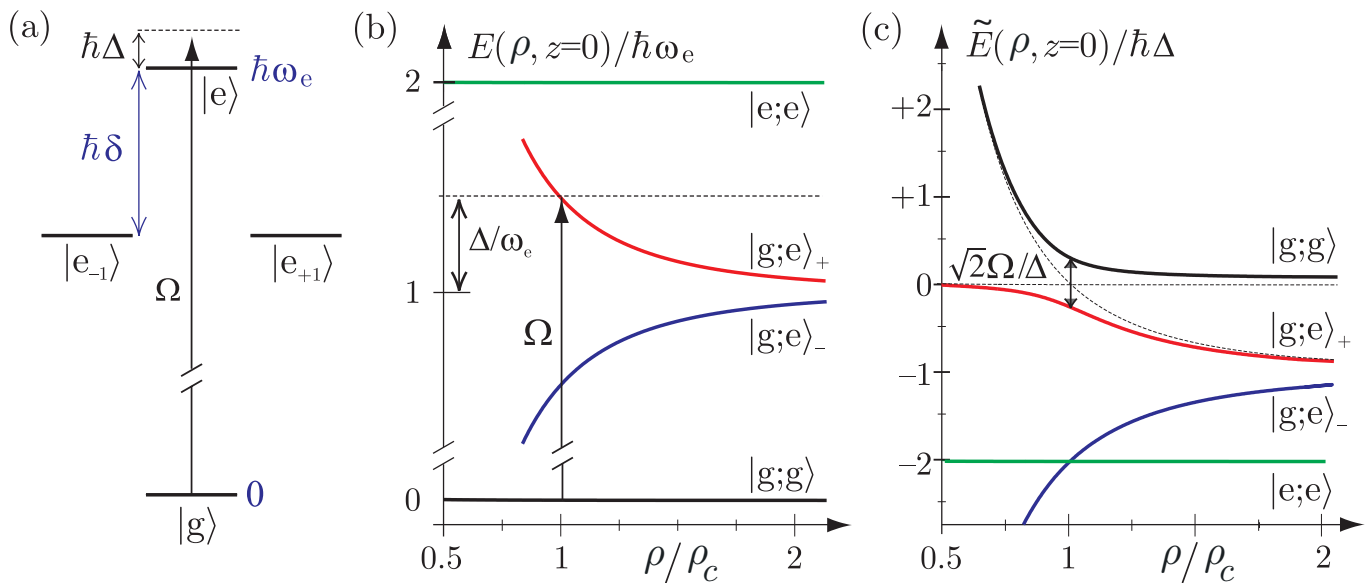


FIG. 3: Design of the step-like potential of Fig. 1(b): (a) Rotational spectrum of a molecule in a weak DC field. The DC field splits the ($J = 1$)-manifold by an amount $\hbar\delta$. The linearly-polarized microwave transition with detuning Δ and Rabi frequency Ω is shown as an arrow. (b) BO-potentials for the internal states for $\Omega = 0$ (bare potentials), where $|g; e\rangle_{\pm} \equiv (|g; e\rangle \pm |e; g\rangle)/\sqrt{2}$. The resonant Condon point ρ_C is indicated by an arrow. (c) AC-field-dressed BO-potentials. The dressed groundstate potential has the largest energy.

don point, an avoided crossing occurs in a *field-dressed* picture, and the new (dressed) groundstate potential inherits the character of the bare ground and excited potentials for distances $\rho \gg \rho_C$ and $\rho \ll \rho_C$, respectively. Consistently, Fig. 3(c) shows that the dressed groundstate potential (which has the *largest* energy) is almost flat for $\rho \gg \rho_C$ and it is strongly repulsive as $1/\rho^3$ for $\rho \ll \rho_C$, which corresponds to the realization of the step-like potential of Fig. 1(b). We remark that, due to the choice of polarization, this strong repulsion is present only in the plane $z = 0$, while for $z \neq 0$ the groundstate potential can turn into attractive. Thus, here the optical confinement along z of Fig. 1(a) is necessary to ensure the stability of the collisional setup.

The interactions in the presence of a single AC field are studied in quite detail in Ref.⁶⁶, where it is shown that in the absence of external confinement, this case is analogous to the (3D) optical blue-shielding developed in the context of ultracold collisions of neutral atoms^{96,97,98}, however with the advantage of the long lifetime of the excited rotational states of the molecules, as opposed to the electronic states of cold atoms. The strong inelastic losses observed in 3D collisions with cold atoms^{96,97,98} can be avoided via a judicious choice of the field's polarization, eventually combined with a tight confinement to a 2D geometry (as e.g. for the case of Fig. 3 above). For example, in Ref.⁹⁹ it is shown that for interactions in the presence of a DC field and of a circularly polarized AC field the *attractive* time-averaged interaction due to the rotating (AC-induced) dipole moments of the molecules allows

for the cancelation of the total dipole-dipole interaction. The residual interactions remaining after this cancelation are *purely repulsive 3D interactions* with a characteristic van-der-Waals behavior $V_{\text{eff}}^{3D}(\mathbf{r}) \sim (d^4/\hbar\Delta)/r^6$. This 3D repulsion provides for a shielding of the inner part of the interaction potential and thus it will strongly suppress inelastic collisions in experiments. This will possibly lead to the realization of quantum degenerate systems of molecules and maybe of tightly-packed crystalline structures in *three-dimensions*⁹⁹.

A cancelation of the leading effective two-body interaction similar to the one sketched above in a *dense* cloud of molecules can lead to the realization of systems where the effective *three-body* interaction $W^{3D}(\mathbf{r}_i, \mathbf{r}_j, \mathbf{r}_k)$ of Eq. (2) dominates over the two-body term $V^{3D}(\mathbf{r}_i - \mathbf{r}_j)$ and determines the groundstate properties of the system. This is interesting, since model Hamiltonians with strong three-body and many-body interactions have attracted a lot of interest in the search for microscopic Hamiltonians exhibiting exotic ground state properties. Well known examples are the fractional quantum Hall states described by the Pfaffian wave functions which appear as ground states of a Hamiltonian with three-body interactions^{100,101,102}. These topological phases admit anyonic excitations with non-abelian braiding statistic. Three-body interactions are also an essential ingredient for systems with a low energy degeneracy characterized by string nets,^{103,104} which play an important role in models for non-abelian topological phases. This possibility of realizing a Hamiltonian where the two-body in-

interaction can be manipulated independently of the three-body term has been studied in Ref.⁸⁹. There, it is shown that a stable system where particles interact via purely repulsive three-body interactions can be realized by combining the setup above with the tight optical confinement provided by an optical lattice. In fact, the latter serves the two-fold purpose of ensuring the collisional stability of the setup and of defining a characteristic length scale (the lattice spacing) where the exact cancelation of the two-body term occurs. The details of this derivation are given in Sect. IV C below, in connection with the derivation of an extended Hubbard model with three-body interactions introduced in the following Sect. IID.

D. Hubbard lattice models

Hubbard Hamiltonians are model Hamiltonians describing the low-energy physics of interacting fermionic and bosonic particles in a lattice¹⁰⁵, and have the general tight-binding form

$$H = - \sum_{i,j,\sigma} J_{ij}^{\sigma} b_{i,\sigma}^{\dagger} b_{j,\sigma} + \sum_{i,j,\sigma,\sigma'} \frac{U_{ij}^{\sigma\sigma'}}{2} n_{i,\sigma} n_{j,\sigma'}. \quad (8)$$

Here $b_{i,\sigma}$ ($b_{i,\sigma}^{\dagger}$) are destruction (creation) operators for a particle at site i in the internal state σ , J_{ij}^{σ} describes the coherent hopping of a particle from site i to site j (typically the nearest neighbor), and $U_{ij}^{\sigma\sigma'}$ describes the onsite ($i = j$) or offsite ($i \neq j$) two-body interactions between particles, with $n_{i,\sigma} = b_{i,\sigma}^{\dagger} b_{i,\sigma}$. Hubbard models have a long history in condensed matter, where they have been used as tight-binding approximations of strongly correlated systems. For example, for particles being electrons in a crystal hopping from the orbital of a given atom to that of its nearest neighbor, σ represents the electron spin. A (fermionic) Hubbard model comprising electrons in a 2D lattice with interspecies onsite interactions is thought to be responsible for the high-temperature superconductivity observed in cuprates¹⁰⁶.

In recent years, Hubbard models have been shown to properly describe the low-energy physics of interacting bosonic and fermionic atoms trapped at the bottom of an optical lattice^{107,108}. The resulting low-energy Hamiltonians are of the form of Eq. (8) above. Spectacular experiments with ultracold atoms have led to the realization of the superfluid/Mott-insulator quantum phase transition for bosonic atoms^{32,33}, and great experimental progresses with fermions promise to solve the phase diagram of the fermionic Hubbard model in 2D by performing an *analog quantum simulation* of Eq. (8) with two-species cold fermions^{109,110}.

Since the interactions between cold atoms are short-ranged, in these systems Hubbard Hamiltonian typically have *onsite* interactions only [$U_{i,i}^{\sigma,\sigma'}$ in Eq. (8)]. However,

it has been shown that the presence of moderately long-range interactions in Eq. (8), such as nearest-neighbor interactions, can lead to interesting phases such as checkerboard solids and 2D supersolids^{87,88}. Polar molecules in optical lattices can provide for offsite interactions^{82,83,84,85,86} which are strong, of the order of hundreds of kHz, and long-range, i.e. they decay with distance as $1/|i - j|^3$. Due to these strong interactions, two molecules cannot hop onto the same site, and thus the particles are treated as effectively "hard-core".

An intriguing possibility is offered by the interaction engineering discussed above in the context of the realization of effective lattice models where particles interact via exotic (extended) Hubbard Hamiltonians. An example of this is given in Ref.⁸⁹, where it is shown how to engineer the following Hubbard-like Hamiltonian

$$H = -J \sum_{\langle ij \rangle} b_i^{\dagger} b_j + \sum_{i \neq j} \frac{U_{ij}}{2} n_i n_j + \sum_{i \neq j \neq k} \frac{W_{ijk}}{6} n_i n_j n_k, \quad (9)$$

where $W_{ijk} n_i n_j n_k$ is an offsite three-body term. The latter is tunable independently of the two-body term $U_{ij} n_i n_j$, to the extent that it can be made to dominate the dynamics and determine the groundstate properties of the system. In contrast to the common approach to derive effective many-body terms from Hubbard models involving two-body interactions, which are obtained in a $J \ll U$ perturbation theory, and are thus necessarily small¹¹¹, the derivation of the Hubbard model Eq. (9) is based directly on the effective many-particle potential Eq. (2). Thus, all the energy scales in Eq. (9) can be tuned independently, which allows to obtain comparatively large hopping rates determining the time and temperature scales to observe exotic quantum phases. This is important, since e.g. in 1D analytical calculations suggest that the Hamiltonian Eq. (9) has a rich groundstate phase-diagram, supporting valence-bond, charge-density-wave and superfluid phases⁸⁹. In Sect. IV below we provide the microscopic derivation of the effective interaction potentials of Eq. (9).

E. Lattice Spin models

The Hamiltonian Eq. (3) can be generalized to include other internal degrees of freedom for each molecule in addition to rotation. This offers new possibilities to engineer effective interactions and novel many-body phases. For example, the addition of a spin-1/2 (qubit) degree of freedom to polar molecules trapped into an optical lattice allows to construct a *complete toolbox* for the simulation of any permutation symmetric lattice spin models⁵⁶. Lattice spin models are ubiquitous in condensed matter physics where they are used as simplified models to describe the characteristic behavior of more complicated interacting physical systems.

The basic building block is a system of two polar molecules strongly trapped at given sites of an optical

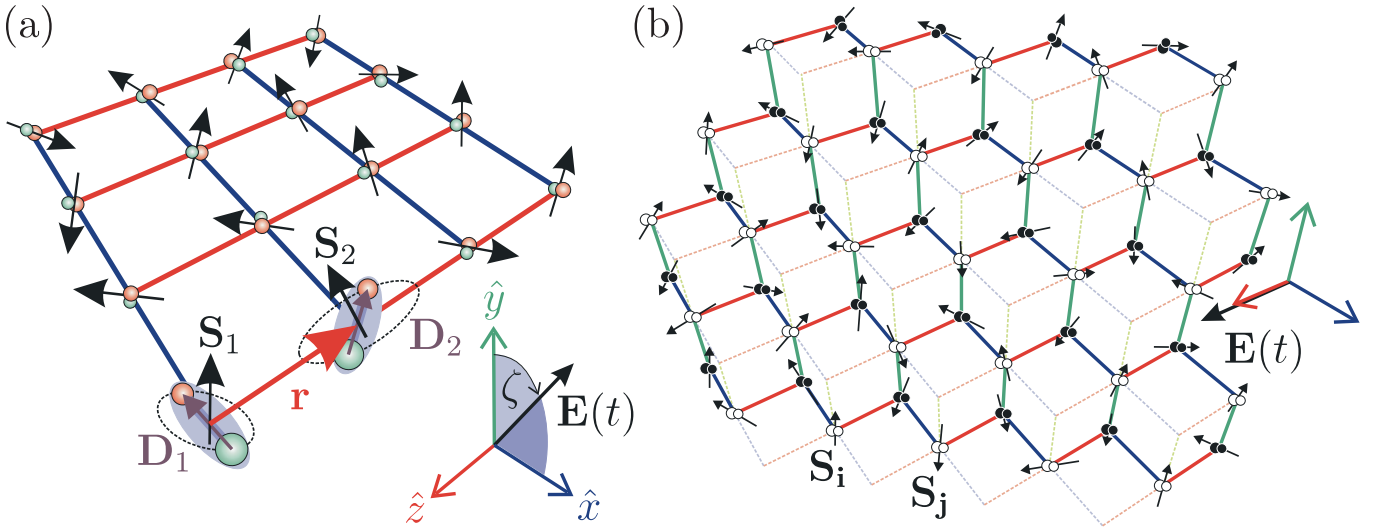


FIG. 4: Example anisotropic spin models that can be simulated with polar molecules trapped in optical lattices. (a) Square lattice in 2D with nearest neighbor orientation dependent Ising interactions along \hat{x} and \hat{z} . Effective interactions between the spins \mathbf{S}_1 and \mathbf{S}_2 of the molecules in their rovibrational ground states are generated with a microwave field $\mathbf{E}(t)$ inducing dipole-dipole interactions between the molecules with dipole moments \mathbf{D}_1 and \mathbf{D}_2 , respectively. (b) Two staggered triangular lattices with nearest neighbors oriented along orthogonal triads. The interactions depend on the orientation of the links with respect to the electric field. (Dashed lines are included for perspective.)

lattice, where the spin-1/2 (or qubit) is represented by a single electron outside a closed shell of a $^2\Sigma_{1/2}$ heteronuclear molecule in its rotational ground state, as provided e.g. by alkaline-earth monohalogenides. As discussed above, heteronuclear molecules have large permanent electric dipole moments, which are responsible for strong, long-range and anisotropic dipole-dipole interactions, whose *spatial dependence* can be manipulated using microwave fields. Accounting for the spin-rotation splitting of molecular rotational levels these dipole-dipole interactions can be made *spin-dependent*. General lattice spin models are then readily built from these binary interactions. Although in this review we will present results for spin-1/2 models only, we notice that the inclusion of hyperfine effects offers extensions to spin systems with larger spin. For example, the design of a large class of spin-1 interactions for polar molecules has been shown in Ref.⁵⁷, which allows e.g. for the realization of a generalized Haldane model in 1D¹¹².

Two highly anisotropic models with spin-1/2 particles that can be simulated are illustrated in Figs. 4(a) and 4(b) respectively. The first takes place on a square 2D lattice with nearest neighbor interactions

$$H_{\text{spin}}^{(\text{I})} = \sum_{i=1}^{\ell-1} \sum_{j=1}^{\ell-1} J(\sigma_{i,j}^z \sigma_{i,j+1}^z + \cos \zeta \sigma_{i,j}^x \sigma_{i+1,j}^x). \quad (10)$$

Introduced by Douçot *et al.*¹¹³ in the context of Josephson junction arrays, this model (for $\zeta \neq \pm\pi/2$) admits a 2-fold degenerate ground subspace that is immune to local noise up to ℓ -th order and hence is a good candidate for storing a protected qubit.

The second, occurs on a bipartite lattice constructed with two 2D triangular lattices, one shifted and stacked on top of the other. The interactions are indicated by nearest neighbor links along the \hat{x} , \hat{y} and \hat{z} directions in real space:

$$H_{\text{spin}}^{(\text{II})} = J_{\perp} \sum_{x\text{-links}} \sigma_j^x \sigma_k^x + J_{\perp} \sum_{y\text{-links}} \sigma_j^y \sigma_k^y + J_z \sum_{z\text{-links}} \sigma_j^z \sigma_k^z. \quad (11)$$

This model has the same spin dependence and nearest neighbor graph as the model on a honeycomb lattice introduced by Kitaev¹¹⁴. He has shown that by tuning the ratio of interaction strengths $|J_{\perp}|/|J_z|$ one can tune the system from a gapped phase carrying abelian anyonic excitations to a gapless phase which in the presence of a magnetic field becomes gapped with non-abelian excitations. In the regime $|J_{\perp}|/|J_z| \ll 1$ the Hamiltonian can be mapped to a model with four body operators on a square lattice with ground states that encode topologically protected quantum memory¹¹⁵. One proposal¹¹⁶ describes how to use trapped atoms in spin dependent optical lattices to simulate the spin model $H_{\text{spin}}^{(\text{II})}$. There the induced spin couplings are obtained via spin dependent collisions in second order tunneling processes. Larger coupling strengths as provided by polar molecules are desirable. In both spin models (I and II) above, the signs of the interactions are irrelevant although one is able to tune the signs if needed.

F. Hubbard models in self-assembled dipolar lattices

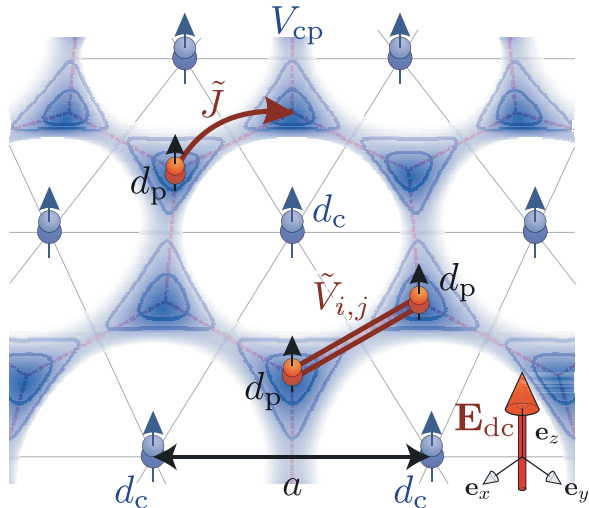


FIG. 5: Floating lattices of dipoles: A self-assembled crystal of polar molecules with dipole moment d_c provides a 2D periodic honeycomb lattice V_{cp} (darker shading corresponds to deeper potentials) for extra molecules with dipole $d_p \ll d_c$ giving rise to a lattice model with hopping \tilde{J} and long-range interactions $\tilde{V}_{i,j}$.

In Hubbard models with cold atoms or molecules in optical lattices there is no phonon degrees of freedom corresponding to an intrinsic dynamics of the lattice, as the back action on the optical potentials is typically negligible. Thus atomic and molecular Hubbard models allow the study of strong correlations in the absence of phonon effects. However, the simulation of models where the presence of (crystal) phonons strongly affects the (Hubbard) dynamics of the particles remains a challenge. These models are of fundamental interest in condensed matter physics, where they describe polaronic and/or superconducting materials¹¹⁸. In the context of atoms, one example is to immerse atoms moving on a lattice into a BEC of a second atomic species, representing a bath of Bogoliubov excitations. A second example is a self-assembled floating lattice of molecules as discussed in Sect. II B, which provides a periodic potential for extra atoms or molecules, whose dynamics can be again described in terms of a Hubbard model⁵⁸. Phonon degrees of freedom enter as vibrations of the dipolar lattice.

The Hamiltonian for extra atoms or molecules in a self-assembled dipolar lattice is

$$H = -J \sum_{\langle i,j \rangle} c_i^\dagger c_j + \frac{1}{2} \sum_{i,j} V_{ij} c_i^\dagger c_j^\dagger c_j c_i + \sum_q \hbar \omega_q a_q^\dagger a_q + \sum_{q,j} M_q e^{i\mathbf{q} \cdot \mathbf{R}_j^0} c_j^\dagger c_j (a_q + a_{-q}^\dagger).$$

Here, the first and second terms define a Hubbard-like Hamiltonian for the extra-particles of the form of Eq. (8),

where the operators c_i (c_i^\dagger) are destruction (creation) operators of the extra-particles. However, the third and fourth terms describe the acoustic phonons of the crystal and the coupling of the extra-particles to the crystal phonons, respectively. Here, a_q destroys a phonon of quansimomentum \mathbf{q} in the mode λ . Tracing over the phonon degrees of freedom in a strong coupling limit provides effective Hubbard models for the extra-particles dressed by the crystal phonons

$$\tilde{H} = -\tilde{J} \sum_{\langle i,j \rangle} c_i^\dagger c_j + \frac{1}{2} \sum_{i,j} \tilde{V}_{ij} c_i^\dagger c_j^\dagger c_j c_i$$

The hopping of a dressed extra-particle between the minima of the periodic potential occurs at a rate \tilde{J} , which is exponentially suppressed due to the co-propagation of the lattice distortion, while offsite particle-particle interactions $\tilde{V}_{i,j}$ are now a combination of direct particle-particle interactions and interactions mediated by the coupling to phonons. The setup we have in mind is depicted in Fig. 6(b), where extra-particles which are molecules with a dipole moment $d_p \ll d_c$ interact repulsively with the crystal molecules, and thus see a periodic (honeycomb) lattice potential.

The distinguishing features of this realization of lattice models are: (i) Dipolar molecular crystals constitute an array of microtraps with its own quantum dynamics represented by phonons (lattice vibrations), while the lattice spacings are tunable with external control fields, ranging from a μm down to the hundred nm regime, i.e. potentially smaller than for optical lattices. (ii) The motion of the extra particles is governed by an interplay of *Hubbard (correlation) dynamics* in the lattice and *coupling to phonons*. The tunability of the lattice allows to access a wide range of Hubbard parameters and phonon couplings. Compared with optical lattices, for example, a small scale lattice yields significantly enhanced hopping amplitudes, which set the relevant energy scale for the Hubbard model, and thus also the temperature requirements for realizing strongly correlated quantum phases.

III. ENGINEERING OF INTERACTION POTENTIALS

In this section we show in some detail how to realize a collisionally stable 2D setup where particles interact via a purely repulsive $1/r^3$ potential, by using a combination of a DC field and of tight optical confinement in the field's direction. We then sketch how to design more complicated interactions using a combination of AC, DC, and optical fields, by focussing on the step-like potential of Fig. 1(b). This engineering of interaction potentials is at the core of the realization of the strongly correlated phases and quantum simulations discussed in Sect. IV below.

A. Molecular Hamiltonian

We consider spin-less polar molecules in their electronic and vibrational ground-state, with spectral notation $X^1\Sigma(0)$. In the following, we are interested in manipulating their rotational states using DC and AC electric fields and in confining their motion using a (optical) far-off-resonance trap (FORT). The application of these external fields will serve as a key element to engineer effective interaction potentials between the molecules.

The low energy effective Hamiltonian for the external motion and internal rotational excitations of a single molecule is

$$H(t) = \frac{\mathbf{p}^2}{2m} + H_{\text{rot}} + H_{\text{DC}} + H_{\text{AC}}(t) + H_{\text{opt}}(\mathbf{r}), \quad (12)$$

where $\mathbf{p}^2/2m$ is the kinetic energy for the center-of-mass motion of a molecule of mass m , H_{rot} accounts for the rotational degrees of freedom, while the terms H_{DC} , $H_{\text{AC}}(t)$ and $H_{\text{opt}}(\mathbf{r})$ refer to the interaction with electric DC and AC (microwave) fields and to the optical trapping of the molecule in the ground electronic-vibrational manifold, respectively. In the following we consider *tight* harmonic optical traps with a frequency $\omega_{\perp} = 2\pi \times 150\text{kHz}$, which is the same for all the relevant rotational states of the molecule. That is, we neglect possible tensor-shifts induced by the optical trapping in the energies of the excited rotational states of the molecules, which in general can be compensated for by an appropriate choice of additional laser fields⁶⁶. Thus, for a confinement along \mathbf{e}_z , $H_{\text{opt}}(\mathbf{r})$ reads $H_{\text{opt}}(\mathbf{r}) = m\omega_{\perp}^2 z^2/2$, independent of the internal (rotational)^{44,119}.

Rotational spectrum :- The term H_{rot} in Eq. (12) is the Hamiltonian for a rigid spherical rotor¹²⁰

$$H_{\text{rot}} = B\mathbf{J}^2, \quad (13)$$

which accounts for the rotation of the internuclear axis of a molecule with total internal angular momentum \mathbf{J} ^{120,121,122}. Rotations are the lowest-energy internal excitations of the molecule. Here B is the rotational constant for the electronic-vibrational ground state, which is of the order of $B \sim h \ 10 \text{ GHz}$ ¹²³. We denote the energy eigenstates of Eq. (13) by $|J, M\rangle$, where J is the quantum number associated with the total internal angular momentum and M is the quantum number associated with its projection onto a *space-fixed* quantization axis. The excitation spectrum is $E_J = BJ(J+1)$, which is anharmonic. Each J -level is $(2J+1)$ -fold degenerate.

A polar molecule has an electric dipole moment, \mathbf{d} , which couples its internal rotational levels and for Σ -molecules is directed along the internuclear axis \mathbf{e}_{ab} , i.e. $\mathbf{d} = d\mathbf{e}_{ab}$. Here, d is the ‘‘permanent’’ dipole moment of a molecule in its electronic-vibrational ground-state. This dipole moment is responsible for the dipole-dipole interaction between two molecules.

The spherical component $d_q = \mathbf{e}_q \cdot \mathbf{d}$ of the dipole operator on the *space-fixed* spherical basis $\{\mathbf{e}_{-1}, \mathbf{e}_0, \mathbf{e}_1\}$, with $\mathbf{e}_{q=0} \equiv \mathbf{e}_z$ and $\mathbf{e}_{\pm 1} = \mp(\mathbf{e}_x \pm i\mathbf{e}_y)/\sqrt{2}$ couples the rotational states $|J, M\rangle$ and $|J \pm 1, M + q\rangle$ according to

$$\begin{aligned} \langle J \pm 1, M + q | d_q | J, M \rangle &= d(J, M; 1, q | J \pm 1, M + q) \times \\ &\times \langle J, 0; 1, 0 | J \pm 1, 0 \rangle \sqrt{\frac{2J+1}{2(J \pm 1) + 1}}, \end{aligned}$$

where $(J_1, M_1; J_2, M_2 | J, M)$ are the Clebsch-Gordan coefficients. This means that for a spherically-symmetric system the eigenstates of the rotor have no net dipole moment, $\langle J, M | \mathbf{d} | J, M \rangle = 0$. However, the dipole coupling to an external electric field breaks this spherical symmetry by aligning each molecule along the field’s direction. This induces a dressing of the rotational energy levels of the molecule, and a corresponding finite dipole moment in each rotational state, as explained below.

Coupling to external electric fields :- The terms H_{DC} and $H_{\text{AC}}(t)$ in Eq.(12) are the electric dipole interaction of a molecule with an external DC electric field $\mathbf{E}_{\text{DC}} = E_{\text{DC}}\mathbf{e}_z$ directed along $\mathbf{e}_0 \equiv \mathbf{e}_z$, and with AC microwave fields $\mathbf{E}_{\text{AC}}(t) = E_{\text{AC}}e^{-i\omega t}\mathbf{e}_q + \text{c.c.}$, which are linearly ($q = 0$) or circularly polarized ($q = \pm 1$) relative to \mathbf{e}_z , respectively. Here we have neglected the spatial dependence of E_{AC} since in the following we are interested in dressing the rotational states of the molecules with microwave fields, whose wavelengths are of the order of centimeters, and thus much larger than the size of our system. Then, the terms H_{DC} and $H_{\text{AC}}(t)$ in Eq. (12) read

$$H_{\text{DC}} = -\mathbf{d} \cdot \mathbf{E}_{\text{DC}} = -d_0 E_{\text{DC}}, \quad (14a)$$

$$H_{\text{AC}}(t) = -\mathbf{d} \cdot \mathbf{E}_{\text{AC}}(t) = -d_q E_{\text{AC}} e^{-i\omega t} + \text{h.c.} \quad (14b)$$

In the presence of a single DC electric field \mathbf{E}_{DC} ($\mathbf{E}_{\text{AC}}, \omega_{\perp}=0$), the internal Hamiltonian is that of a rigid spherical pendulum¹²⁰ $H = H_{\text{rot}} + H_{\text{DC}} = B\mathbf{J}^2 - d_0 E_{\text{DC}}$, which conserves the projection of the angular momentum J on the quantization axis, i.e. M is a good quantum number. Thus, the energy eigenvalues and eigenstates are labeled as $E_{J,M}$ and $|\phi_{J,M}\rangle$, respectively, where each eigenstate $|\phi_{J,M}\rangle$ is a superposition of various states $|J, M\rangle$ mixed by the electric dipole interaction.

The effects of a DC electric field on a single polar molecule are shown in figure Fig. 6, and they amount to: (a) split the $(2J+1)$ -fold degeneracy in the rotor spectrum, and (b) align the molecule along the direction of the field. The latter corresponds to inducing a finite dipole moment in each rotational state. For weak fields $\beta \equiv dE_{\text{DC}}/B \ll 1$, the state $|\phi_{J,M}\rangle$ and its associated

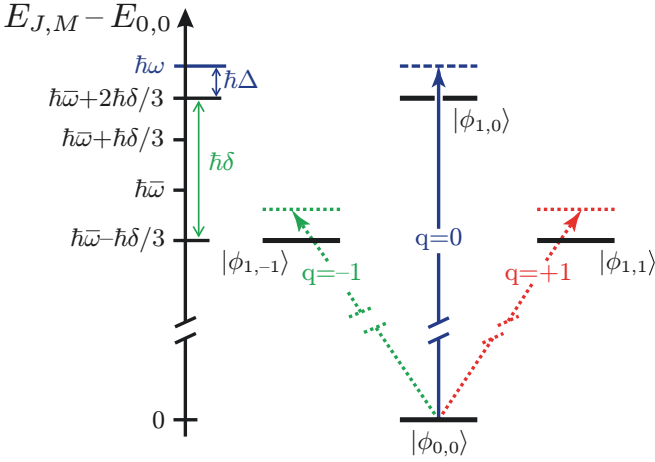


FIG. 6: Solid lines: Energies $E_{J,M}$ (left) and states $|\phi_{J,M}\rangle$ (right) with $J = 0, 1$, for a molecule in a weak DC electric field $\mathbf{E}_{DC} = E_{DC}\mathbf{e}_0$ with $\beta \equiv dE_{DC}/B \ll 1$. The DC-field-induced splitting $\hbar\delta$ and the average energy separation $\hbar\bar{\omega}$ are $\hbar\delta = 3B\beta^2/20$ and $\hbar\bar{\omega} = 2B + B\beta^2/6$, respectively. Dashed and dotted lines: Energy levels for a molecule in combined DC and AC fields (The AC-Stark shifts of the dressed states are not shown). Dashed line: The AC field is monochromatic, with frequency ω , linear polarization $q = 0$, and detuning $\Delta = \omega - (\bar{\omega} + 2\delta/3) > 0$. Dotted lines: Schematics of energy levels for an AC-field with polarization $q = \pm 1$ and frequency $\omega' \neq \omega$.

induced dipole moment approximately read

$$|\phi_{J,M}\rangle = |J, M\rangle - \frac{\beta}{2} \frac{\sqrt{J^2 - M^2}}{\sqrt{J^3(2J+1)}} |J-1, M\rangle + \frac{\beta}{2} \frac{\sqrt{(J+1)^2 - M^2}}{\sqrt{(J+1)^3(2J+1)}} |J+1, M\rangle, \quad (15)$$

and

$$\langle \phi_{J,M} | \mathbf{d} | \phi_{J,M} \rangle = d\beta \frac{3M^2/J(J+1) - 1}{(2J-1)(2J+3)} \mathbf{e}_0,$$

respectively. Thus, the ground state acquires a finite dipole moment $\langle \phi_{0,0} | d_0 | \phi_{0,0} \rangle = d\beta/3$ along the field axis, which is at the origin of ground-state dipole-dipole interactions between polar molecules.

We notice that the for a typical rotational constant, $B \sim h \cdot 10$ GHz, and a dipole-moment $d \sim 9$ Debye the condition $\beta \ll 1$ corresponds to considering DC fields (much) weaker than $B/d \sim 2$ kV/cm.

Individual transitions of the internal Hamiltonian can be addressed by applying one (or several non-interfering) microwave field $\mathbf{E}_{AC}(t)$, which can be *linearly* or *circularly* polarized. This is shown in Fig. 6 for transitions coupling the $J = 0$ and $J = 1$ manifolds, where the Rabi frequency Ω and the detuning Δ are $\Omega \equiv E_{AC}\langle \phi_{1,q} | d_q | \phi_{0,0} \rangle / \hbar$ and $\Delta \equiv \omega - (E_{1,q} - E_{0,0}) / \hbar$, respectively.

Dressed energy levels of a molecule are obtained by diagonalizing the Hamiltonian $H = H_{\text{rot}} + H_{DC} + H_{AC}(t)$ in a Floquet picture. That is, first, the Hamiltonian is expanded on the basis $|\phi_{J,M}\rangle$, which diagonalizes the time-independent part of H as $H_{\text{rot}} + H_{DC} = \sum_{J,M} |\phi_{J,M}\rangle E_{J,M} \langle \phi_{J,M}|$, and then the time-dependent wave-function is expanded in a Fourier series in the AC frequency ω . After applying a rotating wave approximation, i.e. keeping only the energy conserving terms, one obtains a *time-independent* Hamiltonian \tilde{H} , whose eigenvalues correspond to the dressed energy levels⁶⁶.

B. Two molecules

We now consider the interactions of two polar molecules $j = 1, 2$ confined to the $x - y$ plane by a tight harmonic trapping potential of frequency ω_{\perp} , directed along z . The interaction of the two molecules at a distance $\mathbf{r} \equiv \mathbf{r}_2 - \mathbf{r}_1 = r\mathbf{e}_r$ is described by the Hamiltonian

$$H(t) = \sum_{j=1}^2 H_j(t) + V_{\text{dd}}(\mathbf{r}), \quad (16)$$

where $H_j(t)$ is the single-molecule Hamiltonian Eq. (12), and $V_{\text{dd}}(\mathbf{r})$ is the dipole-dipole interaction of Eq. (4).

In the absence of external fields $E_{DC} = E_{AC} = 0$, the interaction of the two molecules in their rotational ground state is determined by the van-der-Waals attraction $V_{\text{vdW}} \sim C_6/r^6$ with $C_6 \approx -d^4/6B$. This expression for the interaction potential is valid outside of the molecular core region $r > r_B \equiv (d^2/B)^{1/3}$, where r_B defines the characteristic length where the dipole-dipole interaction becomes comparable to the splittings of the rotational levels. In the following we show that it is possible to *induce* and *design* interaction potentials which are long-range, by dressing the interactions with appropriately chosen static and/or microwave fields. In fact, the combination of the latter with low-dimensional trapping allows to engineer effective potentials whose *strength* and *shape* can be both tuned. The derivation of the effective interactions proceeds in two steps: (i) We derive a set of Born-Oppenheimer (BO) potentials by first separating Eq. (16) into center-of-mass and relative coordinates, and diagonalizing the Hamiltonian H_{rel} for the relative motion for fixed molecular positions. Within an adiabatic approximation, the corresponding eigenvalues play the role of an effective 3D interaction potential in a given state manifold dressed by the external field. (ii) We eliminate the motional degrees of freedom in the tightly confined z direction to obtain an effective 2D dynamics with interaction $V_{\text{eff}}^{2D}(\boldsymbol{\rho})$.

In the following we show how to design interaction potentials, presenting in some details the simplest case of a purely repulsive $1/r^3$ potential in 2D, obtained using a static electric field (Sect. III B 1). We then sketch how to design more elaborate potentials using a combination

of static and microwave fields coupling the lowest rotor states of each molecule (Sect. III B 2).

1. Designing the repulsive $1/r^3$ potential in 2D

Collisions in a DC field:- We consider a weak static electric field applied in the z -direction $\mathbf{E} = E_{\text{DC}}\mathbf{e}_0$ with $\beta = dE_{\text{DC}}/B \ll 1$, and in the absence of optical trapping ($\omega_{\perp} = 0$). The effective interaction potentials for the collision of the two particles can be obtained in the adiabatic approximation by neglecting the kinetic energy and by diagonalizing the following Hamiltonian H_{rel} for fixed particle positions

$$\begin{aligned} H_{\text{rel}} &= \sum_{j=1}^2 [B\mathbf{J}_j^2 - E_{\text{DC}}d_{0,j}] + V_{\text{dd}}(\mathbf{r}) \\ &= \sum_n |\Phi_n(\mathbf{r})\rangle E_n(\mathbf{r}) \langle \Phi_n(\mathbf{r})|, \end{aligned} \quad (17)$$

where $E_n(\mathbf{r})$ and $|\Phi_n(\mathbf{r})\rangle$ are the n th adiabatic energy eigenvalues and two-particle eigenfunctions, respectively. In the limit $r \rightarrow \infty$ the latter are symmetrized products of the single-particle states $|\phi_{J_j, M_j}\rangle_j$ of Eq. (15), while for finite r they are superpositions of several single-particle states, which are mixed by the dipole-dipole interaction $V_{\text{dd}}(\mathbf{r})$. The quantity $n \equiv (J; M; \sigma)$ is the collective quantum number labeling the eigenvalues $E_n(\mathbf{r})$, with $J = J_1 + J_2$ the total number of rotational excitations shared by the two molecules, $M \equiv |M_1| + |M_2|$ the total projection of angular momentum onto the electric field direction, and $\sigma = \pm$ the permutation symmetry associated with the exchange of the two particles. We note that, because of the presence of the DC field, here J is a simple label for the various energy manifolds, and not a quantum number.

Since we are mainly interested in ground-state collisions, in the following we restrict our discussion to the $J_j = 0$ and 1 manifolds of each molecule, which amounts to taking into account 16 rotational two-particle states. Figure 7 shows the corresponding eigenvalues $E_n(\mathbf{r})$ as a function of the interparticle distance r , for $\beta = 1/5$. The vector \mathbf{r} is expressed in spherical coordinates $\mathbf{r} = (r, \vartheta, \varphi)$, with ϑ and φ the polar and azimuthal angles, respectively, and $z = r \cos \vartheta$. Figure 7(a) shows that the energy spectrum has a markedly different behavior in the molecular core region $r < r_B$ and for $r > r_B$, with $r_B \equiv (d^2/B)^{1/3}$. In fact, for $r < r_B$ the energy spectrum is characterized by a series of level crossings and anti-crossings, which make the satisfaction of the adiabatic approximation generally impossible. For $r > r_B$ the energy levels group into well-defined manifolds, which are approximately spaced by an energy $2B$, corresponding to a quantum of rotational excitation. In the following we focus on this region $r > r_B$, where the adiabatic approximation can be fulfilled.

Figures 7(b,c) and Figs. 7(d,e) are blow-ups of the two lowest-energy manifolds of Fig. 7(a) in the region $r > r_B$,

for $\vartheta = \pi/2$ and $\vartheta = 0$, respectively. Figure. 7(b) and Fig. 7(d) show that the excited state manifold with one quantum of rotation ($J_1 + J_2 = 1$) is asymptotically split into two sub-manifolds. This separation corresponds to the electric-field-induced splitting of the $J_j = 1$ manifold of each molecule, and it is thus given by $\hbar\delta = 3B\beta^2/20$, see caption of Fig. 6. More importantly, Figs. 7(c) and (e) show that the effective ground-state potential $E_0(\mathbf{r})$ has a very different character for the cases $\vartheta = \pi/2$ and $\vartheta = 0$, respectively. In fact, in the case $\vartheta = \pi/2$ [Fig. 7(c)], corresponding to collisions in the ($z = 0$)-plane, the potential is attractive for $r < r_*$, while for $r > r_*$ it turns into repulsive and it decays at large distances as $1/r^3$, where r_* is a characteristic length to be defined below. On the other hand, for $\vartheta = 0$ [see Fig. 7(e)] the potential is purely attractive, with dipolar character. This change in character of the ground-state potential as a function of ϑ is captured by the following analytic expression for $E_{0;0,+}(\mathbf{r})$, as derived in perturbation theory in $V_{\text{dd}}(\mathbf{r})/B$,

$$V_{\text{eff}}^{3\text{D}}(\mathbf{r}) \equiv E_{0;0,+}(\mathbf{r}) \approx \frac{C_3}{r^3} (1 - 3 \cos^2 \vartheta) + \frac{C_6}{r^6}. \quad (18)$$

Here, the constants $C_3 \approx d^2\beta^2/9$ and $C_6 \approx -d^4/6B$ are the dipolar and van-der-Waals coefficients for the ground-state, respectively, and the constant term $2E_{0,0} = -\beta^2 B/3$ due single-particle DC Stark-shifts has been neglected. Equation (18) is valid for $r \gg r_B$ and $V_{\text{dd}}(\mathbf{r})/B \ll 1$, and it shows that the potential $V_{\text{eff}}^{3\text{D}}(\mathbf{r})$ has a local maximum in the plane $z = r \cos \vartheta = 0$ at the position r_* , defined as

$$r_* \equiv \left(\frac{2|C_6|}{C_3} \right)^{1/3} \approx \left(\frac{3d^2}{B\beta^2} \right)^{1/3}, \quad (19)$$

where the dipole-dipole and van-der-Waals interactions become comparable. The height of this maximum is

$$V_* = \frac{C_3^2}{4|C_6|} \approx \frac{B\beta^4}{54}, \quad (20)$$

and the curvature of the potential along z [$\partial_z^2 V(r = r_*, z = 0) = -6C_3/r_*^5 \equiv -m\omega_c^2/2$] defines a characteristic frequency

$$\omega_c \equiv \left(\frac{12C_3}{mr_*^5} \right)^{1/2}, \quad (21)$$

to be used below. The latter has a strong dependence $\beta^{8/3} = (dE_{\text{DC}}/B)^{8/3}$ on the applied electric field. For distances $r \gg r_*$ the dipole-dipole interaction dominates over the van-der-Waals attractive potential, and $V_{\text{eff}}^{3\text{D}}(\mathbf{r}) \sim C_3(1 - 3 \cos^2 \vartheta)/r^3$, see Ref.⁵⁰. Thus, if it were possible to confine the collisional dynamics to the ($z = 0$)-plane with $r \gg r_*, r_B$, purely repulsive long-range interactions with a characteristic dipolar spatial dependence $\sim 1/r^3$ could be attained. In the following we analyze the conditions for realizing this setup, using a strong confinement along z as provided,

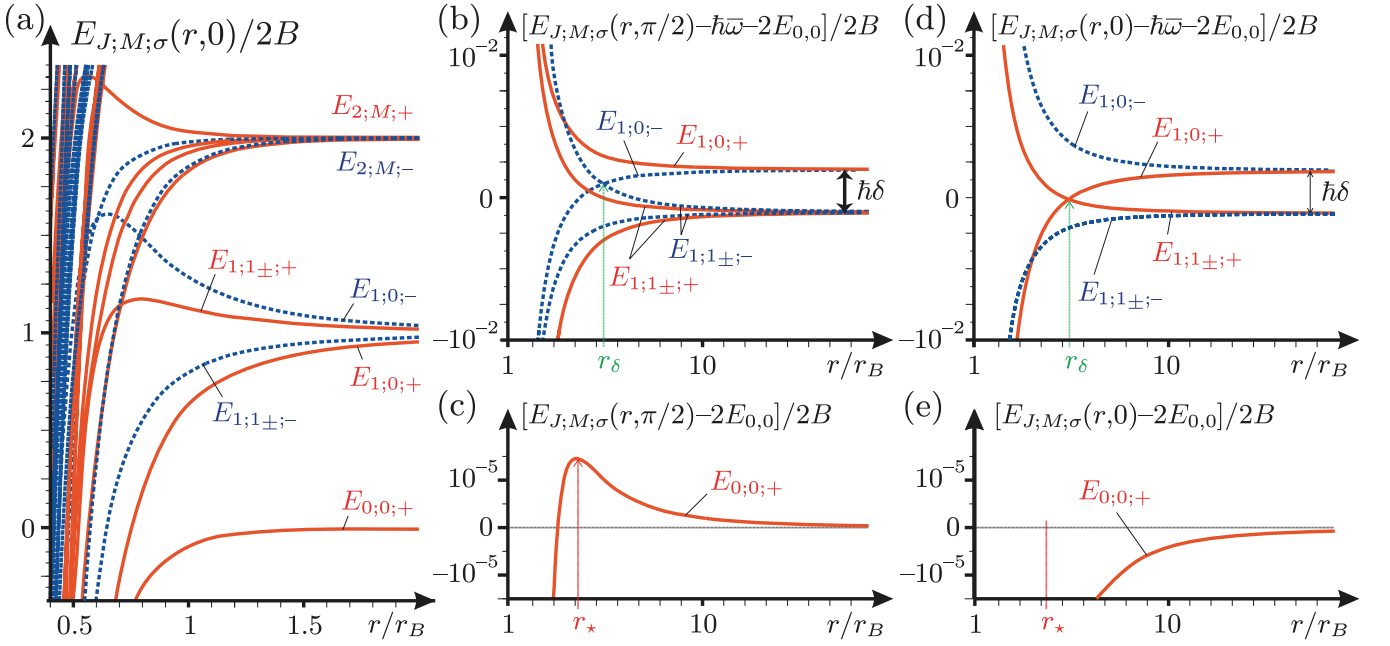


FIG. 7: BO-potentials $E_{J;M;\sigma}(r, \vartheta)$ for two molecules colliding in the presence of a DC field, with $\beta \equiv dE_{\text{DC}}/B = 1/5$. The solid and dashed curves correspond to symmetric ($\sigma = +$) and antisymmetric ($\sigma = -$) eigenstates, respectively. (a): BO-potentials for the 16 lowest-energy eigenstates $E_{J;M;\sigma}(r, \vartheta)$. The molecular-core region is identified as the region $r < r_B = (d^2/B)^{1/3}$, while for $r \gg r_B$ the eigenstates group into manifolds separated by one quantum of rotational excitation $2B$. (b) and (d): Blow-ups of the first-excited energy manifold of panel (a) in the region $r \gtrsim r_B$ for $\vartheta = \pi/2$ and $\vartheta = 0$, respectively. Note the electric-field-induced splitting $\hbar\delta \equiv 3B\beta^2/20$. The distance r_δ where the dipole-dipole interaction becomes comparable to $\hbar\delta$ is $r_\delta = (d^2/\hbar\delta)^{1/3}$. (c) and (e): Blow-ups of the ground-state potential $E_{0,0,+}(r, \vartheta)$ of panel (a) in the region $r \gtrsim r_B$ for $\vartheta = \pi/2$ and $\vartheta = 0$, respectively. The distance r_* of Eq. (19), where the dipole-dipole interaction becomes comparable to the van-der-Waals attraction is indicated. Note the repulsive (attractive) character of the potential for $\vartheta = \pi/2$ ($\vartheta = 0$) and $r > r_*$.

e.g. by an optical trapping potential.

Parabolic confinement :- The presence of a finite trapping potential of frequency ω_\perp in the z -direction provides for a position-dependent energy shift of Eq. (18). The new potential reads

$$V(\mathbf{r}) = \frac{C_3}{r^3} (1 - 3 \cos^2 \vartheta) + \frac{C_6}{r^6} + \frac{1}{4} m \omega_\perp^2 z^2. \quad (22)$$

As noted before, for $z = 0$ the repulsive dipole-dipole interaction dominates over the attractive van-der-Waals at distances $r \gg r_*$ given in Eq. (19). In addition, for $\omega_\perp > 0$ the harmonic potential confines the particle's motion in the z direction. Thus, the combination of the dipole-dipole interaction and of the harmonic confinement yields a repulsive potential which provides for a *three-dimensional* barrier separating the long-distance from the short-distance regime. If the collisional energy is much smaller than this barrier, the particle's motion is confined to the long-distance region, where the potential is purely repulsive.

Figure 8 is a contour plot of $V(\mathbf{r})$ in units of V_* , for $\beta > 0$ and $\omega_\perp = \omega_c/10$, with $\mathbf{r} \equiv (\rho, z) = r(\sin \vartheta, \cos \vartheta)$ (the angle φ is neglected due to the cylindrical symmetry of the problem). Darker regions correspond to

a stronger repulsive potential, while the white region at $\rho \approx 0$ is the short-range, attractive part of the potential. The repulsion due to the dipole-dipole and harmonic potentials is distinguishable at $|z|/r_* \sim 0$ and 7, respectively. The lesser-dark regions located at $(\rho_\perp, \pm z_\perp) \equiv \ell_\perp(\sin \vartheta_\perp, \pm \cos \vartheta_\perp)$ correspond to the existence of two saddle points positioned in between the maxima of $V(\mathbf{r})$, with $\ell_\perp = (12C_3/m\omega_\perp^2)^{1/5}$ and $\cos \vartheta_\perp = \sqrt{1 - (r_*/\ell_\perp)^3}/\sqrt{5}$, [see circles in Fig. 8]. These saddle points act as an effective potential barrier separating the attractive part of the potential present at $r < \ell_\perp$ from the region $r \gg \ell_\perp \geq r_*, r_B$ where the effective interaction potential Eq. (22) is purely repulsive. For collisional energies smaller than the height of this barrier the dynamics of the particles can be reduced to a *quasi* two-dimensional (2D) dynamics, by tracing over the fast particle motion in the z -direction. We notice that the existence of two saddle points at distances $r \sim \ell_\perp$ separating the long- from the short-distance regimes is a general feature of systems with a comparatively weak transverse trapping $\omega_\perp/\omega_c < 1$, with ω_c defined in Eq. (21). In fact, for a strong transverse trapping $\omega_\perp \geq \omega_c$ the two saddle points collapse into a single one located at $z = 0$, and $\rho = \ell_\perp \sim r_*$. In this limit the dynamics is purely 2D, with the particles

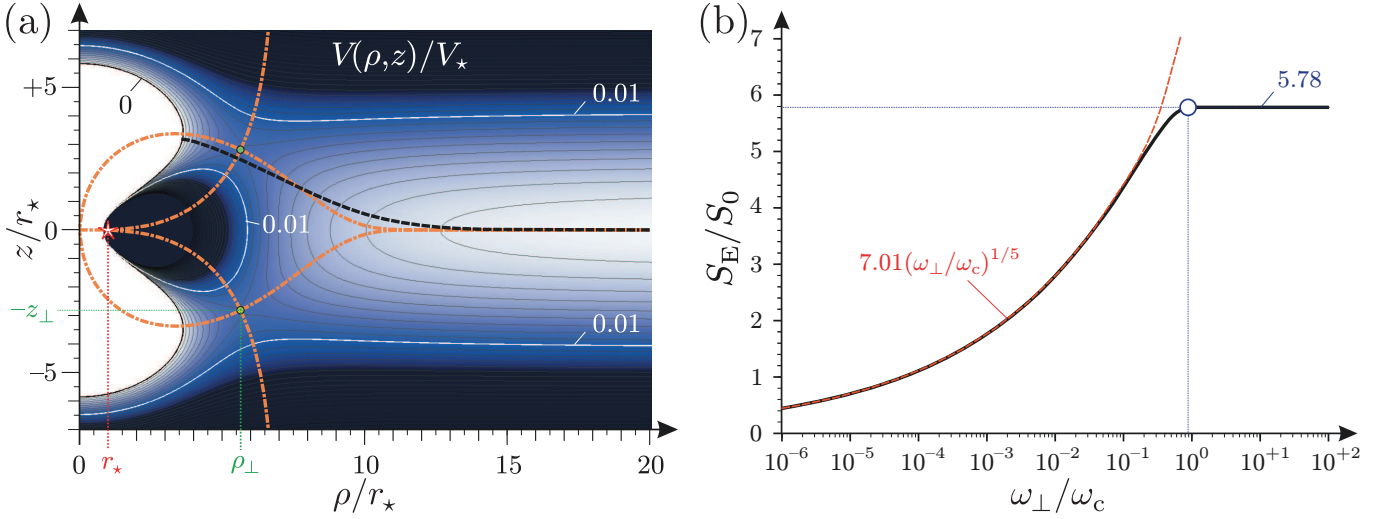


FIG. 8: (a) Contour plot of the effective potential $V(\rho, z)$ of Eq. (22), for two polar molecules interacting in the presence of a DC field $\beta > 0$, and a confining harmonic potential in the z -direction, with trapping frequency $\omega_{\perp} = \omega_c/10$, where $\omega_c \equiv (12C_3/mr_*^5)^{1/2}$ of Eq. (21) and $r_* = (2|C_6|/C_3)^{1/3}$ of Eq. (19). The contour lines are shown for $V(\rho, z)/V_* \geq 0$, with $V_* = B\beta^4/54$. Darker regions represent stronger repulsive interactions. The combination of the dipole-dipole interactions induced by the DC field and of the harmonic confinement leads to realizing a 3D repulsive potential. The repulsion due to the dipole-dipole interaction and of the harmonic confinement is distinguishable at $z \sim 0$ and $z/r_* \sim \pm 7$, respectively. Two saddle points (circles) located at $(\rho_{\perp}, \pm z_{\perp})$ separate the long-distance region where the potential is repulsive $\sim 1/r^3$ from the attractive short-distance region. The gradients of the potential are indicated by dash-dotted lines. The thick dashed line indicates the instanton solution for the tunneling through the potential barrier. (b) The euclidian action S_E as a function of ω_{\perp}/ω_c (solid line). For $\omega_{\perp} < \omega'_c \approx 0.88 \omega_c$ ($\omega_{\perp} > \omega'_c$) the "bounce" occurs for $z(0) \neq 0$ (within the plane $z(0) = 0$), see text. The point ω'_c is signaled by a circle. For $\omega_{\perp} > \omega'_c$ the action is $S_E \approx 5.78 S_0$, with $S_0 = \sqrt{m|C_6|}/\hbar r_*^2$, which is ω_{\perp} -independent, consistent with the "bounce" occurring in the ($z = 0$)-plane (see text).

strictly confined to the ($z = 0$)-plane.

Collisional stability :- When an ensemble of polar molecules is considered, inelastic collisions and three body recombination may lead the system to a potential instability, associated with the attractive character of the dipole-dipole interaction^{67,68,69,70,71,72,73,74,75}. In our discussion, this instability is associated with the population of the short-distance region $r < \ell_{\perp}$, which can be efficiently suppressed for strong dipole-dipole interactions and transverse confinement. In fact, for collisional energies smaller than the potential barrier $V(\rho_{\perp}, \pm z_{\perp})$ the particles are mostly confined to the long-distance regime, where they scatter elastically. That is, when a cold ensemble of molecules is considered the barrier provides for the stability of the system by "shielding" the short-distance attractive part of the two-body potential. In this limit, residual losses are due to the tunneling through the potential barrier at a rate Γ , which can be efficiently suppressed for reasonable values of β and ω_{\perp} , as shown below.

The tunneling rate $\Gamma = \Gamma_0 e^{-S_E/\hbar}$ through the barrier $V(\rho_{\perp}, \pm z_{\perp})$ can be calculated using a semiclassical/instanton approach¹²⁴. The euclidian action S_E , which is responsible for the exponential suppression

of the tunneling, is plotted in Fig. 8 as a function of ω_{\perp}/ω_c , in units of $S_0 = \sqrt{m|C_6|}/r_*^2$. The figure shows that S_E has different behaviors for $\omega_{\perp} \ll \omega_c$ and $\omega_{\perp} \gg \omega_c$. In fact, for $\omega_{\perp} \ll \omega_c$ the action increases with increasing ω_{\perp} as $S_E \approx 7.01 S_0 (\omega_{\perp}/\omega_c)^{1/5} = 1.43 \hbar (\ell_{\perp}/a_{\perp})^2$ (dotted line), which depends on the confinement along z , via $a_{\perp} = (\hbar/m\omega_{\perp})^{1/2}$. On the other hand, for $\omega_{\perp} \gg \omega_c$ it reads $S_E \approx 5.78 S_0$, which is ω_{\perp} -independent. The transition between the two different regimes mirrors the change in the nature of the underlying potential $V(\mathbf{r})$. In particular, for $\omega_{\perp} \gtrsim \omega_c$ the dynamics is strictly confined to the plane $z = 0$ and thus it becomes independent of ω_{\perp} . The constant Γ_0 is related to the quantum fluctuations around the semiclassical trajectory, and its value is strongly system-dependent. For the crystalline phase of Ref.⁵⁰, it is the collisional "attempt frequency", proportional to the characteristic phonon frequency $\Gamma_0 \sim \sqrt{C_3/m} a^{-5}$, with a the mean interparticle distance.

In the limit of strong interactions and tight transverse confinement Γ rapidly tends to zero. We illustrate this for the example of SrO, which has a permanent dipole-moment of $d \approx 8.9$ Debye and mass $m = 104$ amu. Then, for a tight transverse optical lattice with harmonic oscillator frequency $\omega_{\perp} = 2\pi \times 150$ kHz and for a DC-field $\beta = dE_{DC}/B = 1/3$ we have $(C_3^2 m^3 \omega_{\perp}/8\hbar^5)^{1/5} \approx 3.39$

and we obtain $\Gamma/\Gamma_0 \approx e^{-5.86 \times 3.39} \approx 2 \times 10^{-9}$. Even for a DC field as weak as $\beta = 1/6$ we still obtain a suppression by five order of magnitudes, as $\Gamma/\Gamma_0 \approx e^{-5.86 \times 1.94} \approx 10^{-5}$. This calculation confirms that a collisionally stable setup for polar molecules in the strongly interacting regime can be realized by combining the strong dipole-dipole interactions with a tight transverse confinement.

Effective 2D interaction:- The effective two-dimensional interaction potential is obtained by integrating out the fast particle motion in the transverse direction z . For $r > \ell_\perp \gg a_\perp$, the two-particle eigenfunctions in the z -direction approximately factorize into products of single-particle harmonic oscillator wavefunctions $\psi_{k_1}(z_1)\psi_{k_2}(z_2)$, and in first order perturbation theory in $V_{\text{eff}}^{2D}/\hbar\omega_\perp$ the effective 2D interaction potential V_{eff}^{2D} reads

$$V_{\text{eff}}^{2D}(\boldsymbol{\rho}) \approx \frac{1}{\sqrt{2\pi}a_\perp} \int dz e^{-z^2/2a_\perp^2} V_{\text{eff}}^{3D}(\mathbf{r}). \quad (23)$$

For large separations $\rho \gg \ell_\perp$ the 2D potential reduces to

$$V_{\text{eff}}^{2D}(\boldsymbol{\rho}) = \frac{C_3}{\rho^3},$$

which is a purely repulsive 2D interaction potential. The derivation of $V_{\text{eff}}^{2D}(\boldsymbol{\rho})$ is one of the central results of this section. We show below (Sect. IV) that the use of this interaction potential leads to the realization of interesting many-body phases, in the context of condensed matter applications using cold molecular quantum gases.

2. Designing *ad-hoc* potentials with AC-fields

Above we have shown how to design 2D effective groundstate interactions which are purely repulsive and decay as $\sim 1/r^3$. The use of one or several non interfering AC fields allows to engineer more complicated interactions by combining the spatial texture of the adiabatic groundstate potential of the two-particle spectrum with that of selected excited potentials, in a dressed picture. This mixing of ground and excited-state potentials is favored by the dipole-dipole interactions which split the degeneracy of the excited-state manifolds of the two-particle spectrum and render the state-selectivity of the AC fields *space-dependent*, as explained below. In combination with a strong optical confinement, and due to the long lifetimes of the excited rotational states¹²⁵, this allows for the realization of collisionally stable setups for molecules in the strongly interacting regime.

We exemplify the situation above by considering the case of a single AC field $\mathbf{E}_{\text{AC}}(t) = E_{\text{AC}} e^{-i\omega t} \mathbf{e}_q + \text{c.c.}$ which is added to the configuration of Fig. 7 (interactions in the presence of a static electric field $\mathbf{E}_{\text{DC}} = \beta B \mathbf{e}_z$). The field's polarization is chosen to be linear ($q = 0$)

and the frequency ω is blue-detuned from the ($|\phi_{0,0}\rangle \rightarrow |\phi_{1,0}\rangle$)-transition of the single-particle spectrum by an amount $\Delta = \omega - 2B/\hbar > 0$. The effects of the AC-field on the two-particle scattering can be summarized as: (a) Inducing *oscillating* dipole-moments in each molecule, which determine long-range dipole-dipole interactions [in addition to those determined by the static field \mathbf{E}_{DC}], whose sign and angular dependence are given by the polarization q ; (b) Inducing a coupling of the ground and excited state manifolds of the *two-particle* spectrum at a resonant (Condon) point $r_C = (d^2/3\hbar\Delta)^{1/3}$, where the dipole-dipole interaction becomes comparable to the detuning Δ . This coupling is responsible for an avoided crossing of the *field-dressed* energy levels at r_C , whose properties depend crucially on the polarization q . This fact is at the core of the engineering of interaction potentials, in that the 3D effective *dressed adiabatic* ground-state interaction potential inherits the character of the bare ground and excited potentials for $r \gg r_C$ and $r \ll r_C$, respectively.

The setup above is illustrated in Fig. 9(a) and (b), where the continuous and dashed lines are the bare ($\mathbf{E}_{\text{AC}} = 0$) symmetric and anti-symmetric potentials $E_{J;M;\sigma}(\mathbf{r})$ of Fig. 7, respectively, and the presence of the AC-field is signaled by a black arrow at the resonant Condon point r_C . The presence of the weak DC field splits asymptotically the ($J = 1$)-manifold by an amount $\hbar\delta$ as in Fig. 7(b), allowing for a simple fulfillment of the adiabatic approximation in the excited-state manifold for distances $r \gg r_\delta = (d^2/\hbar\delta)^{1/3}$. In fact, the energy of the $E_{1;0,+}(\mathbf{r})$ potential becomes degenerate with the energy of other bare symmetric potentials only at distances $r \ll r_\delta$. In addition, we notice that the presence of the splitting $\hbar\delta$ also shifts the level crossing with antisymmetric states to small distances $r \ll r_\delta$.

For distances $r \gg r_\delta = (d^2/\hbar\delta)^{1/3}$, we are allowed to consider only the four states of Fig. 9(b), since all the other potentials of the ($J = 1$)- and ($J = 2$)-manifolds are far detuned by an amount which is (at least) of order $\delta \gg \Delta$ and they are not coupled by the AC-field to the bare ground state $E_{0,0,+}(\mathbf{r})$, due to the choice of field's polarization. Figure 9(b) shows that the splitting induced by the dipole-dipole interaction in the ($J = 1$)-manifold renders the detuning Δ position-dependent, so that at r_C the energy of the bare ground-state and that of the symmetric bare excited state become degenerate. The resulting dressed ground-state potential is sketched in Fig. 9(b) (thick black line) and it roughly corresponds to the bare $E_{0,0,+}(\mathbf{r})$ and $E_{1,0,+}(\mathbf{r})$ potentials for $r > r_C$ and $r < r_C$, respectively. Accordingly, Fig. 9(c) shows that the dressed groundstate potential $\tilde{E}_{0,0,+}(\mathbf{r})$, which has the *highest energy*, turns from weakly to strongly repulsive for $r \gg r_C$ and $r \ll r_C$, respectively. This change in the character of the ground-state interaction potential corresponds to the design of a "step-like" interaction. This example shows that the 3D ground-state interaction for two molecules can be strongly modified by the combined use of AC and DC fields, which is

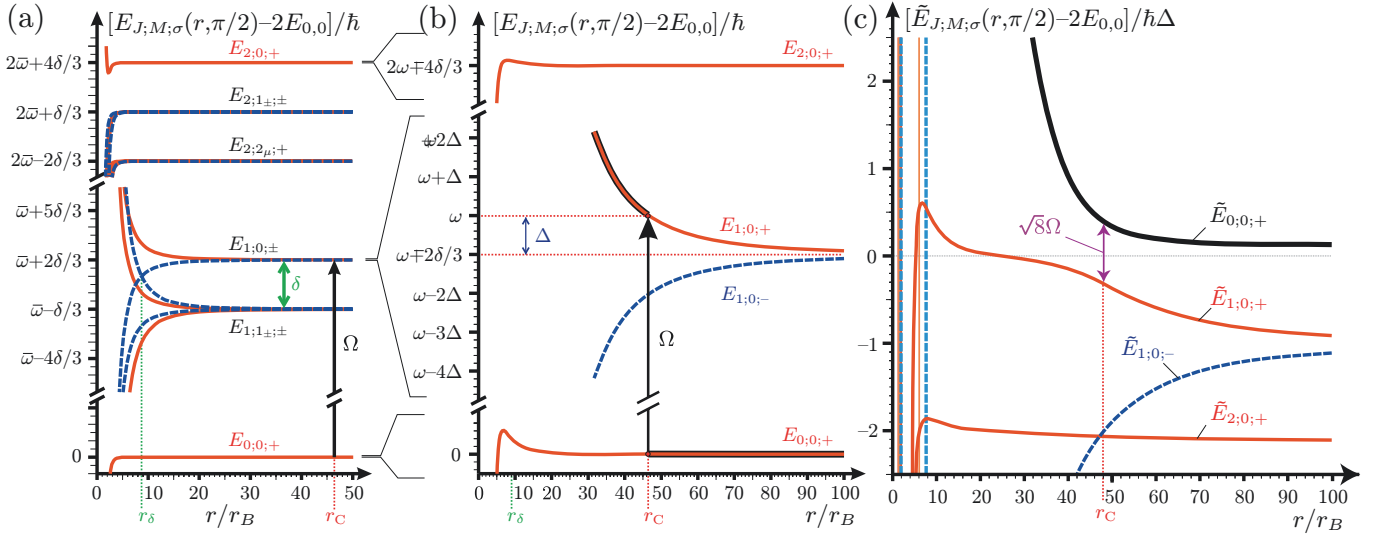


FIG. 9: (a) Schematic representation of the effects of a DC and an AC microwave fields on the interaction of two molecules. The solid and dashed lines are the bare potentials $E_n(\mathbf{r}) \equiv E_{J;M;\sigma}(r, \vartheta)$ of Sect. IIIB 1 with $\vartheta = \pi/2$ for interactions in the presence of the DC field only, for the symmetric ($\sigma = +$) and antisymmetric ($\sigma = -$) states, respectively. The DC field induces a splitting $\hbar\delta$ of the first-excited manifold of the two-particle spectrum. A microwave-field of frequency $\omega = \bar{\omega} + 2\delta/3 + \Delta$ is blue detuned by $\Delta > 0$ from the single-particle rotational resonance. The dipole-dipole interaction further splits the excited-state manifold, making the detuning space-dependent. Eventually, the combined energy of the bare ground-state potential $E_{0,0,+}(\mathbf{r})$ and of an AC photon (black arrow) becomes degenerate with the energy of the bare symmetric $E_{1,0,+}(r, \pi/2)$. The resonant point $r_C = (d^2/3\hbar\Delta)^{1/3}$ occurs at $r \approx 46 r_B$. (b) Blow-up of the potentials of panel (a) with $M = 0$. The dressed ground-state potential is sketched by a thick solid line. (c) The four potentials of panel (b) in the field-dressed picture. The dressed ground-state potential $\tilde{E}_{0,0,+}(r, \pi/2)$ has the largest energy and is indicated by a thick solid line.

the central result of this section. More complicated potentials can be engineered using multiple AC fields and different polarizations.

Analogous to the case ($\mathbf{E}_{AC} = 0$) of Sect. IIIB 1, the interaction potential of Fig. 9 is actually repulsive along certain directions (e.g. $\theta = \pi/2$, as shown in the figure), while it turns into attractive along others (e.g. $\theta = 0$, not shown). As for the ($\mathbf{E}_{AC} = 0$)-case of Sect. IIIB 1, when more than two particles are considered this attraction can lead to many-body instabilities. Moreover, here the dressed potential $\tilde{E}_{0,0,+}(\mathbf{r})$ of Fig. 9(c) is *not* the lowest-energy potential, which in general can introduce additional loss channels. The latter correspond to diabatic couplings to symmetric states for particles approaching distances $r \lesssim r_C$, and are therefore present even in the simple *two-particle* collisional process, and to couplings to anti-symmetric states, which can be induced e.g. by three-body collisions or by non-compensated tensor-shifts for two optically-trapped particles. The presence of all of these loss channels may render impractical the realization of collisionally stable setups for strongly interacting molecular gases (although Ref.⁹⁹ for a solution involving the use of a *circularly* polarized AC field). However, we have seen above that for the setup of Fig. 9 the presence of the static field shifts the various resonance points with the potentials which are responsible for these loss channels *in the* ($\vartheta = \pi/2$)-*plane* ($z = 0$) to distances

$r \ll r_C$. This suggests that by confining the particles motion *to the plane* $z = 0$ by using a strong optical transverse confinement analogous to that of Sect. IIIB 1 it is possible to realize collisionally stable setups in the region $r > r_C$. This scheme has been shown to work in Ref.⁶⁶ and thus the main message here is that a judicious combination of the dipole-dipole interactions and of the optical confinement can act as an effective "shield" of the region $r < r_C$ where losses occur and thus the collisional setup can be made stable. The use of the step-like potential above and of other engineered potentials can lead to the realization of interesting phases for an ensemble of polar molecules in the *strongly interacting regime*^{50,66}.

IV. MANY-BODY PHYSICS WITH COLD POLAR MOLECULES

A. 2D Self-Assembled crystals

The above discussion of the intermolecular potentials and of the stability of collisional setups in reduced dimensionality provides the microscopic justification for studying an ensemble of polar molecules in 2D interacting *via* (modified) dipole-dipole potentials. At low temperatures $T < \hbar\omega_{\perp}$, the general *many body Hamiltonian* has the form of Eq. (5). As an example of the possibilities offered by potential engineering to realize novel many-body

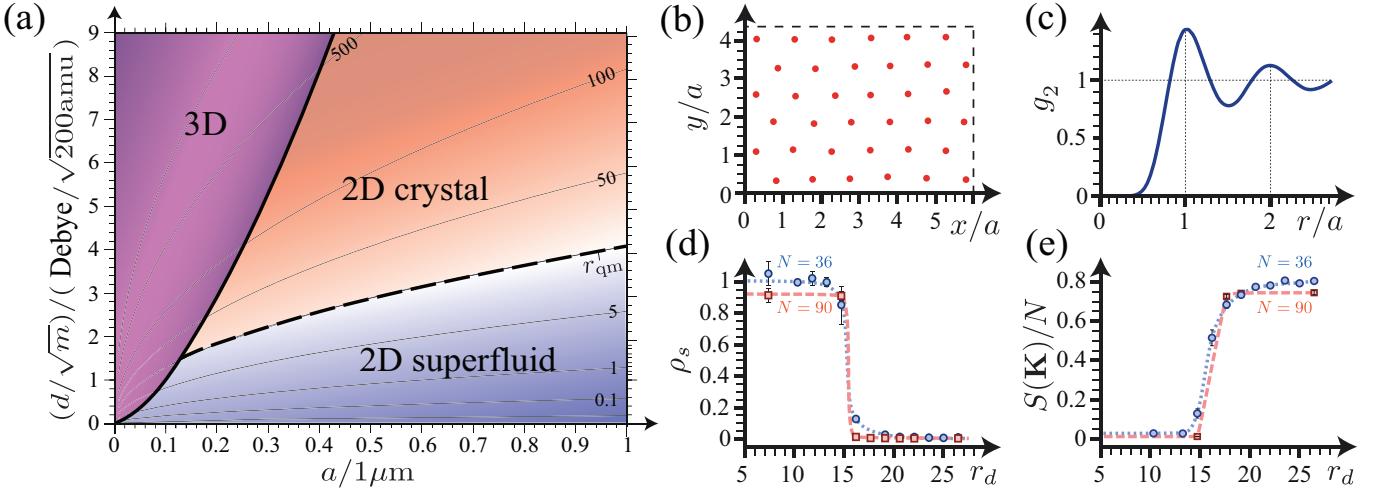


FIG. 10: (a) Quantum phases of 2D dipoles: Contour plot of the interaction strength $r_d = Dm/\hbar^2 a$ as a function of the dipole moment d (in Debye) and of the interparticle distance a (in μm), with m the mass of a molecule (in atomic units $200\times\text{amu}$). The regions of stability of the 2D superfluid and crystalline phases where $\hbar\omega_\perp > D/a^3$ are indicated, with $\omega_\perp = 2\pi \times 150\text{kHz}$ the frequency of the transverse confinement. (b) PIMC-snapshot of the mean particle positions in the crystalline phase for $N = 36$ at $r_d \approx 26.5$. (c) Density-density (angle-averaged) correlation function $g_2(r)$, for $N = 36$ at $r_d \sim 11.8$. (d) Superfluid density ρ_s and (e) static structure factor $S(\mathbf{K})/N$ as a function of r_d , for $N = 36$ (circles) and $N = 90$ (squares).

quantum phases, we here focus on bosonic particles interacting via the effective potential

$$V_{\text{eff}}^{2\text{D}}(\rho) = D/\rho^3 \quad (24)$$

derived in Sect. III B 1. This is the simplest attainable interaction potential, and thus the one which is experimentally most interesting in the short term. However, despite the simplicity of the interaction potential, the Hamiltonian Eq. (5) gives rise to novel quantum phenomena, which have not been accessed so far in the context of cold neutral atoms and molecules. In particular, by means of Path Integral Monte-Carlo simulations (PIMC), in Ref.⁵⁰ we show the appearance of a *self-assembled* crystalline phase and an associated quantum melting transition into a superfluid as a function of the interaction strength r_d . As explained in Sect. II, the latter is the ratio

$$r_d = \frac{Dm}{\hbar^2 a} \quad (25)$$

between the interaction energy D/a^3 and the kinetic energy \hbar^2/ma^2 at the mean interparticle distance a , with m the mass of a molecule.

In Fig. 2(a) a tentative phase diagram is sketched for the two-dimensional system of bosonic dipoles. In the limit of weak interactions $r_d < 1$, the ground state is a superfluid (SF) with a finite (quasi) condensate. The SF is characterized by a superfluid fraction $\rho_s(T)$, which depends on temperature T , with $\rho_s(T=0) = 1$. Since we consider a 2D setup, a Berezinskii–Kosterlitz–Thouless transition towards a normal fluid is expected to occur at a finite temperature $T_{\text{KT}} = \pi\rho_s\hbar^2 n/2m$. In the opposite

limit of strong interactions $r_d \gg 1$ the polar molecules are in a crystalline phase for temperatures $T < T_m$ with $T_m \approx 0.09D/a^3 \simeq 0.018r_d E_{\text{R,c}}$, while for larger temperature the crystal melts into a normal fluid via a first-order (classical) phase transition. The critical value T_m for this melting transition has been obtained via molecular dynamics simulations in the context of interfacial colloidal crystals in Ref.⁹⁴. Here, $E_{\text{R,c}} \equiv \pi^2\hbar^2/2ma^2$ is the crystal recoil energy, typically a few to tens of kHz. The configuration with minimal energy is thus a triangular lattice with spacing $a_L = (4/3)^{1/4}a$. Excitations of the crystal are acoustic phonons with Hamiltonian

$$H_c = \sum_q \hbar\omega_q a_q^\dagger a_q, \quad (26)$$

where a_q destroys a phonon of quasimomentum \mathbf{q} in the mode λ . The characteristic Debye frequency is $\hbar\omega_D \sim 1.6\sqrt{r_d}E_{\text{R,c}}$. At $T = 0$ the static structure factor S diverges at a reciprocal lattice vector \mathbf{K} , and thus $S(\mathbf{K})/N$ acts as an order parameter for the crystalline phase.

In Ref.⁵⁰ we investigated the intermediate strongly interacting regime with $r_d \gtrsim 1$, and we determined the critical interaction strength r_{QM} for the quantum phase transition between the superfluid and the crystal. In our analysis we used a recently developed PIMC-code based on the Worm algorithm⁹⁵, which is an *exact* Monte-Carlo method for the determination of thermodynamic quantities in continuous space at small finite temperature. In Fig. 10(d-e), the order parameters ρ_s and $S(\mathbf{K})/N$ are shown at a small temperature $T = 0.014D/a^3$ for different interaction strengths r_d and particle numbers $N = 36, 90$. We find that ρ_s exhibits a sudden drop

to zero for $r_d \approx 15$, while at the same position $S(\mathbf{K})$ strongly increases. In addition, during the Monte-Carlo simulations we observed that in a few occasions ρ_s suddenly jumped from 0 to 1, and then returned to 0, in the interval $r_d \approx 15 - 20$, which suggests a competition between the superfluid and crystalline phases. These results indicate a superfluid to crystal phase transition at

$$r_{\text{QM}} = 18 \pm 4. \quad (27)$$

The step-like behavior of ρ_s and $S(\mathbf{K})/N$ is consistent with a first order phase transition, a result which has been confirmed in Refs.^{51,52}. We notice that the superfluid with $r_d \sim 1$ is strongly interacting, and in particular the density-density correlation function is quenched on lengths $R < a$, see Fig. 10(c). This observation is consistent with the validity condition of the effective 2D interaction potential Eq. (24), that two particles never approach each other at distances smaller than l_\perp .

Having determined the low-temperature phase-diagram, the remaining question is whether these phases, and in particular the crystalline phase emerging at strong dipole-dipole interactions, are in fact accessible with polar molecules. This question is addressed in Fig. 10(a), which is a contour plot of the interaction strength r_d as a function of the induced dipole moment $d = \sqrt{D}$ (in units of Debye) and of the mean interparticle distance a (in μm). The dimensionless quantity $\sqrt{m/200amu}$ depends on the mass m of the molecules (in atomic units), and it is of order one for characteristic molecules like SrO or RbCs. In the figure, stable 2D configurations for the molecules exist in the parameter region where the transverse (optical) trapping frequency $\omega = 2\pi \times 150\text{Hz}$ exceeds the dipole-dipole interaction ($\hbar\omega > D/a^3$), such that $l_\perp = (12D/m\omega_\perp^2)^{1/5} < a$, consistent with the stability discussion of Sect. III B 1 [notice that $l_\perp \sim (D/\hbar\omega_\perp)^{1/3}$ for realistic parameters]. The figure shows that for a given induced dipole d the ground-state of an ensemble of polar molecules is a crystal for mean interparticle distances $l_\perp \lesssim a \lesssim a_{\text{max}}$, where $a_{\text{max}} \equiv d^2 m / \hbar^2 r_{\text{QM}}$ corresponds to the distance at which the crystal melts into a superfluid. For SrO (RbCS) molecules with permanent dipole moment $d = 8.9D$ ($d = 1.25D$), $a_{\text{min}} \sim 200\text{nm}$ (100nm), while a_{max} can be several μm . Since for large enough interactions the melting temperature T_m can be of order of several μK , the self-assembled crystalline phase should be accessible for reasonable experimental parameters using cold polar molecules.

For what concerns the observability of the zero-temperature phases, Bragg scattering with optical light allows for probing the crystalline phase, while the detection of vortices can be used as a definitive signature of superfluidity. We notice that the 2D (quasi) condensate involves a fraction of the total density only, and therefore we expect only small coherence peaks in a time of flight experiment.

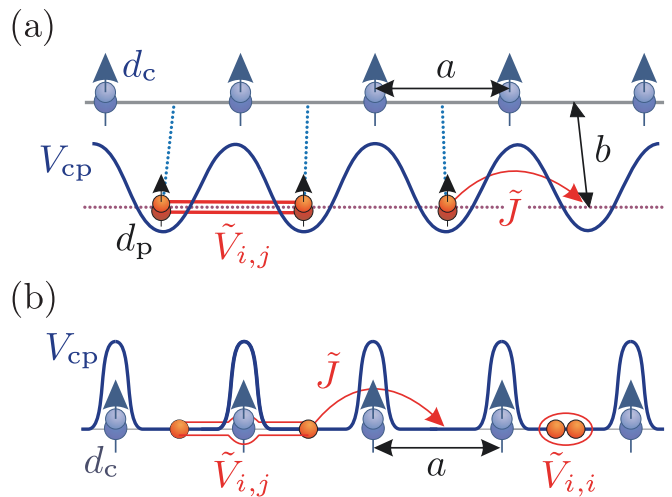


FIG. 11: A dipolar crystal of polar molecules provides a periodic lattice V_{cp} for extra atoms or molecules giving rise to a lattice model with hopping \tilde{J} and long-range interactions $\tilde{V}_{i,j}$ (see text and Fig. 5). (a) A 1D dipolar crystal with lattice spacing a provides a periodic potential for a second molecular species moving in a parallel tube at distance b (Configuration 1). (b) 1D setup with atoms scattering from the dipolar lattice (Configuration 2).

Finally, we notice that by adding an additional *in-plane* optical confinement, it is possible to realize strongly interacting 1D phases which are analogous to the 2D crystals discussed above^{53,54,55}. For large enough interactions $r \gg 1$, the phonon frequencies have the simple form $\hbar\omega_q = (2/\pi^2) [12r_d f_q]^{1/2} E_{\text{R,c}}$, with $f_q = \sum_{j>0} 4 \sin(qaj/2)^2 / j^5$. The Debye frequency is $\hbar\omega_{\text{D}} \equiv \hbar\omega_{\pi/a} \sim 1.4\sqrt{r_d} E_{\text{R,c}}$, while the classical melting temperature can be estimated to be of the order of $T_m \simeq 0.2r_d E_{\text{R,c}} / k_B$, see Ref.⁵⁵.

B. Floating lattices of dipoles

An interesting possibility offered by the realization of the self-assembled crystals discussed above is to utilize them as floating mesoscopic lattice potentials to trap extra-particles, which can be atoms or polar molecules of a different species. We show below that within an experimentally accessible parameter regime extended Hubbard models with tunable long-range phonon-mediated interactions describe the effective dynamics of the extra-particles dressed by the lattice phonons.

The setups that we have in mind are shown in Figs. 5 and 11(a-b) where extra particles confined to a 2D crystal plane or a 1D tube scatter from the periodic lattice potential $\sum_j V_{\text{cp}}(\mathbf{R}_j - \mathbf{r})$. Here, \mathbf{r} and $\mathbf{R}_j = \mathbf{R}_j^0 + \mathbf{u}_j$ are the coordinates of the particle and crystal molecule j , respectively, with \mathbf{R}_j^0 the equilibrium positions and \mathbf{u}_j small displacements. For particles being molecules, this

potential is given by the repulsive dipole-dipole interaction $V_{\text{cp}}(\mathbf{R}_j - \mathbf{r}) = d_p d_c / |\mathbf{R}_j - \mathbf{r}|^3$ with $d_p \ll d_c$ the induced dipole moment, and for atoms we assume that the interaction is modeled by a short range pseudopotential proportional to an elastic scattering length a_{cp} . In addition, extra molecules and atoms will interact according to dipolar, or short range interactions, respectively.

We are interested in a situation where the extra particles in the lattice are described by a single band Hubbard Hamiltonian coupled to the acoustic phonons of the lattice¹²⁶

$$H = -J \sum_{\langle i,j \rangle} c_i^\dagger c_j + \frac{1}{2} \sum_{i,j} V_{ij} c_i^\dagger c_j^\dagger c_j c_i + \sum_{q,j} M_q e^{i\mathbf{q}\cdot\mathbf{R}_j^0} c_j^\dagger c_j (a_q + a_{-q}^\dagger) + H_c. \quad (28)$$

The first and second terms describe the nearest neighbor hopping of the extra particles with hopping amplitudes J , and interactions V , computed for each microscopic model by band-structure calculations for $\mathbf{u}_j = 0$, respectively. The operators c_i (c_i^\dagger) are destruction (creation) operators of the particles. The third term is the phonon coupling obtained in lowest order in the displacement

$$\mathbf{u}_j = i \sum_q (\hbar/2m_c N \omega_q)^{1/2} \xi_q (a_q + a_{-q}^\dagger) e^{i\mathbf{q}\cdot\mathbf{R}_j^0},$$

with

$$M_q = \bar{V}_{\mathbf{q}} \cdot \xi_q (\hbar/2N m_c \omega_q)^{1/2} \beta_{\mathbf{q}}.$$

Here, ξ_q and N are the phonon polarization and the number of lattice molecules, respectively, while $\bar{V}_{\mathbf{q}}$ is the Fourier transform of the particle-crystal interaction V_{cp} , and $\beta_{\mathbf{q}} = \int d\mathbf{r} |w_0(\mathbf{r})|^2 e^{i\mathbf{q}\cdot\mathbf{r}}$, with $w_0(\mathbf{r})$ the Wannier function of the lowest Bloch band¹²⁶. The validity of the single band Hubbard model requires $J, V < \Delta$, and temperatures $k_B T < \Delta$ with Δ the separation to the first excited Bloch band.

The Hubbard parameters of Eq. (28) are of the order of magnitude of the recoil energy, $J, V \sim E_{\text{R},c}$, and thus (much) smaller than the Debye frequency $\hbar\omega_D \sim E_{\text{R},c} \sqrt{r_d}$, for $r_d \gg 1$ ¹²⁷. This separation of time scales $J, V \ll \hbar\omega_D$, combined with the fact that the coupling to phonons is dominated by high frequencies $\hbar\omega > J, V$ (see the discussion of M_q below) is reminiscent of polarons as particles dressed by (optical) phonons, where the dynamics is given by coherent and incoherent hopping on a lattice^{118,126}. This physical picture is brought out in a master equation treatment within a strong coupling perturbation theory. The starting point is a Lang-Firsov transformation of the Hamiltonian $H \rightarrow SHS^\dagger$ with a density-dependent displacement

$$S = \exp \left[- \sum_{q,j} \frac{M_q}{\hbar\omega_q} e^{i\mathbf{q}\cdot\mathbf{R}_j^0} c_j^\dagger c_j (a_q - a_{-q}^\dagger) \right].$$

This eliminates the phonon coupling in the second line of Eq. (28) in favor of a transformed kinetic energy term

$$-J \sum_{\langle i,j \rangle} c_i^\dagger c_j X_i^\dagger X_j,$$

where the displacement operators

$$X_j = \exp \left[\sum_q \frac{M_q}{\hbar\omega_q} e^{i\mathbf{q}\cdot\mathbf{R}_j^0} (a_q - a_{-q}^\dagger) \right]$$

can be interpreted as a lattice recoil of the dressed particles in a hopping process. In addition, the bare interactions are renormalized according to

$$\tilde{V}_{ij} = V_{ij} + V_{ij}^{(1)},$$

with $V_{ij}^{(1)} = -2 \sum_q \cos(\mathbf{q}(\mathbf{R}_i^0 - \mathbf{R}_j^0)) M_q^2 / \hbar\omega_q$, that is, the phonon couplings induce and modify off-site interactions. The onsite interaction is given by $\tilde{V}_{j,j} = V_{j,j} - 2E_p$ with

$$E_p = \sum_q \frac{M_q^2}{\hbar\omega_q}$$

the *polaron* self-energy or *polaron shift*. For $J = 0$ the new Hamiltonian is diagonal and describes interacting polarons and independent phonons. The latter are vibrations of the lattice molecules around new equilibrium positions with unchanged frequencies. A stable crystal requires the variance of the displacements Δu around these new equilibrium positions to be small compared to a .

A Born-Markov approximation with the phonons a finite temperature heatbath with $J, V \ll \hbar\omega_D$ (see above), and the transformed kinetic energy

$$-J \sum_{\langle i,j \rangle} c_i^\dagger c_j (X_i^\dagger X_j - \langle\langle X_i^\dagger X_j \rangle\rangle)$$

as the system-bath interaction with $\langle\langle X_i^\dagger X_j \rangle\rangle$ the equilibrium bath average, provides the master equation for the reduced density operator of the dressed particles ρ_t in Lindblad form¹²⁸

$$\dot{\rho}_t = \frac{i}{\hbar} [\rho_t, \tilde{H}] + \sum_{j,l,\delta,\delta'} \frac{\Gamma_{j,l}^{\delta,\delta'}}{2\hbar} ([b_{j\delta}, \rho_t b_{l\delta'}] + [b_{l\delta'}, \rho_t b_{j\delta}]), \quad (29)$$

with $b_{j\delta} = c_{j+\delta}^\dagger c_j$. The effective system Hamiltonian

$$\tilde{H} = -\tilde{J} \sum_{\langle i,j \rangle} c_i^\dagger c_j + \frac{1}{2} \sum_{i,j} \tilde{V}_{ij} c_i^\dagger c_j^\dagger c_j c_i, \quad (30)$$

is of the extended Hubbard type, valid for $\tilde{J}, \tilde{V}_{ij}, E_p < \Delta$. For $E_p > \Delta$, Eq.(3) should be derived via a multi-band approach. *Coherent* hopping of the dressed particles is described by

$$\tilde{J} = J \langle\langle X_i^\dagger X_j \rangle\rangle \equiv J \exp(-S_T),$$

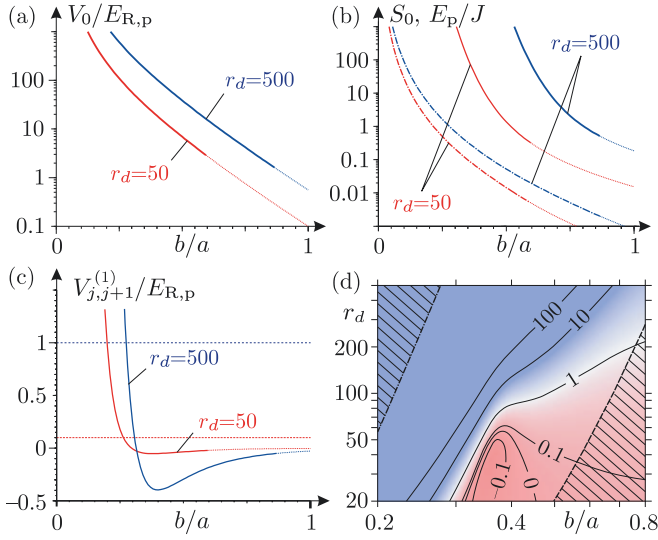


FIG. 12: Configuration 1 [Fig. 11(a)]: Hubbard parameters for $d_p/d_c = 0.1$ and $m = m_p$. (a) Lattice depth V_0 in units of $E_{R,p}$ vs. b/a for $r_d = 50$ and 500. Thick continuous lines: tight-binding region $4J < \Delta$. (b) Reduction factor S_0 (dashed dotted lines) and polaron shift E_p/J (solid lines), for $4J < \Delta$. (c) Continuous lines: phonon-mediated interactions $V_{j,j+1}^{(1)}$. Horizontal (dashed) lines: $V_{j,j+1}$. (d) Contour plot of $\tilde{V}_{j,j+1}/2\tilde{J}$ (solid lines) as a function of b/a and r_d . A single-band Hubbard model is valid left of the dashed region ($4J, \tilde{V}_{ij} < \Delta$), and right of the black region ($E_p < \Delta$).

where

$$S_T = \sum_q \left(\frac{M_q}{\hbar\omega_q} \right)^2 [1 - \cos(\mathbf{q}\mathbf{a})](2n_q(T) + 1)$$

characterizes the strength of the particle-phonon interactions, and $n_q(T)$ is the thermal occupation at temperature T ¹²⁶.

The dissipative term in Lindblad form in Eq. (29) corresponds to thermally activated *incoherent* hopping with rates $\Gamma_{j,l}^{\delta,\delta'}$, which can be made negligible for the energies of interest $k_B T \ll \min(\Delta, E_p, k_B T_C)$, see Refs.^{118,129}. Corrections to Eq. (30) proportional to J^2 are small relative to \tilde{H} provided $J \ll E_p$ ¹¹⁸ (also $J \ll \hbar\omega_D$ in 1D^{129,130}). Thus, in the parameter regime of interest the dynamics of the dressed particles is described by the extended Hubbard Hamiltonian \tilde{H} . In the following, we verify the existence of this parameter regime and we calculate the effective Hubbard parameters from the microscopic model for the 1D configuration of Fig. 11(a), where extra-particles are polar molecules of a different species. An analogous calculation for the configuration of Fig. 11(b) is reported in Ref.⁵⁸.

In the configuration of Fig. 11(a) molecules of a second species are trapped in a tube at a distance b from the

crystal tube under 1D trapping conditions. For crystal molecules fixed at the equilibrium positions with lattice spacing a , the extra particles feel a periodic potential

$$V_{cp}(x) = d_c d_p \sum_j [b^2 + (x - ja)^2]^{-3/2},$$

which determines the bandstructure. The lattice depth

$$V_0 \equiv V_{cp}(a/2) - V_{cp}(0) \sim r_d \frac{d_p}{d_c} \frac{m_p}{m} \frac{e^{-3b/a}}{(b/a)^3} E_{R,p}$$

is shown in Fig. 12(a) as a function of b/a , where the thick solid lines indicate the parameter regime $4J < \Delta$, and $E_{R,p} = \hbar^2 \pi^2 / 2m_p a^2$. The potential is comb-like for $b/a < 1/4$, since the particles resolve the individual molecules forming the crystal, while it is sinusoidal for $b/a \gtrsim 1/4$. The strong dipole-dipole repulsion between the extra particles acts as an effective hard-core constraint⁸⁹. We find that for $4J < \Delta$ and $d_p \ll d_c$ the bare off-site interactions satisfy

$$V_{ij} \sim d_p^2 / (a|i-j|)^3 < \Delta,$$

which justifies a single-band approximation for the dynamics of the extra-particles in the static potential.

The particle-phonon coupling is

$$M_q = \frac{d_c d_p}{ab} \left(\frac{2\hbar}{Nm_c \omega_q} \right)^{1/2} q^2 \mathcal{K}_1(b|q|) \beta_q$$

with \mathcal{K}_1 the modified Bessel function of the second kind, and $M_q \sim \sqrt{q}$ for $q \rightarrow 0$. In the regime of interest $b/a < 1$ where the single-band approximation is valid ($4J, V_{ij} < \Delta$), we find that M_q is peaked at large $q \sim \pi/a$, so that the main contribution to the integrals in the definition of S_T and E_p is indeed dominated by large frequencies $\hbar\omega_q > J$. Together with the separation of time-scales $J, V_{ij} \ll \hbar\omega_D$, this is consistent with the picture of the system's dynamics as given by particles dressed by *fast* (optical) phonons, as discussed above. We notice that this so-called *anti-adiabatic* regime is generally hard to achieve in cold atomic setups¹²⁷.

A plot of S_0 as a function of b/a is shown in Fig. 12(b). We find the scaling

$$S_0 \propto \sqrt{r_d} (d_p/d_c)^2,$$

and within the regime of validity of the single band approximation, S_0 can be tuned from $S_0 \ll 1$ ($\tilde{J} \sim J$) to $S_0 \gg 1$ ($\tilde{J} \ll J$) corresponding to the large and small polaron limit, respectively. The polaron shift E_p generally exceeds the bare hopping rate J , and in particular, $E_p \gg J$ for $S_0 \gtrsim 1$, see Fig. 12(b). Together with the condition $\hbar\omega_D \gg J$ this ensures that the corrections to Eq.(30) which are proportional to J^2 are indeed small, and thus Eq.(30) fully accounts for the coherent dynamics of the dressed particles.

The extended Hubbard model corresponding to the configuration of Fig 11(a) is characterized by tunable off-site interactions, which are a combination of the direct

dipole-dipole interactions between the extra-particles and of the phonon-mediated interactions $V_{i,j}^{(1)}$. For $b/a \lesssim 1/4$ we find that the interactions $V_{i,j}^{(1)}$ decay slowly with the inter-particle distance as $\sim 1/|i-j|^2$, and are thus long-ranged. The sign of $V_{i,j}^{(1)}$ is a function of the ratio b/a . Thus, depending on b/a the phonon-mediated interactions can enhance or reduce the direct dipole-dipole repulsion of the extra particles. As an example, Fig. 12(c) shows that the sign of the term $V_{j,j+1}^{(1)}$ alternates between attractive and repulsive as a function of b/a , and that for small enough b/a the phonon-mediated interactions can become larger than the direct dipole-dipole interactions.

The effective Hubbard parameters $\tilde{V}_{j,j+1}$ and \tilde{J} are summarized in Fig. 12(d), which is a contour plot of $\tilde{V}_{j,j+1}/2\tilde{J}$ as a function of r_d and b/a . The ratio $\tilde{V}_{j,j+1}/2\tilde{J}$ increases by decreasing b/a or increasing r_d , and can be much larger than one. This appearance of strong off-site interactions in the effective dynamics is a necessary ingredient for the realization of a variety of new quantum phases^{82,83,84,85,86}. As an example of the possible quantum phases that can be realized in this setup, at half filling, and considering nearest-neighbor interactions only, the particles in the configuration described above undergo a transition from a (Luttinger) liquid ($\tilde{V}_{i,i+1} < 2\tilde{J}$) to a charge-density-wave ($\tilde{V}_{i,i+1} > 2\tilde{J}$) as a function of b/a and r_d . Figure 12(d) shows that the parameter regime $\tilde{V}_{i,i+1} \approx 2\tilde{J}$, see Ref.¹³¹, where this transition occurs can be satisfied for various choices of r_d and b/a , e.g. for $r_d = 100$ and $b/a \approx 0.5$.

C. Three-body interactions

As discussed in Sect. II, it is of interest to design systems where effective many-body interactions dominate over the two-body interactions, and determine the properties of the groundstate. We here describe how an effective low energy interaction potential V_{eff} of the form Eq. (2) can be derived in the Born-Oppenheimer approximation for $^1\Sigma$ polar molecules interacting via dipole-dipole interactions by dressing low lying rotational states of each molecule with external static and microwave fields, in analogy to the discussion of Sect. III B.

We here focus on a setup with a static electric field $\mathbf{E} = E\mathbf{e}_z$ along the z -axis, see Fig. 13, where the two states $|g\rangle_i \equiv |\phi_{0,0}\rangle_i$ and $|e_+\rangle_i \equiv |\phi_{1,+1}\rangle_i$ with energies E_g and $E_{e,\pm}$ are coupled by a circularly polarized microwave field propagating along the z -axis. The microwave transition is characterized by the (blue) detuning $\Delta > 0$ and the Rabi frequency Ω/\hbar . While the following discussion can be readily generalized to include the degenerate case⁸⁹, here we assume that the degeneracy of the states $|e_-\rangle \equiv |\phi_{1,-1}\rangle_i$ and $|e_+\rangle_i$ is lifted, e.g., by an additional microwave field coupling the state $|e_-\rangle$ near-resonantly to the next state manifold, see Fig. 13. Then, the internal structure of a single polar molecule reduces to a

two-level system and is described as a spin-1/2 particle via the identification of the state $|g\rangle_i$ ($|e_+\rangle_i$) as eigenstate of the spin operator S_i^z with positive (negative) eigenvalue. In the rotating frame and applying the rotating wave approximation, the Hamiltonian describing the internal dynamics of the polar molecule reduces to

$$H_0^{(i)} = \frac{1}{2} \begin{pmatrix} \Delta & \Omega \\ \Omega & -\Delta \end{pmatrix} = \mathbf{h}\mathbf{S}_i \quad (31)$$

with the effective magnetic field $\mathbf{h} = (\Omega, 0, \Delta)$ and the spin operator $\mathbf{S}_i = (S_i^x, S_i^y, S_i^z)$. The eigenstates of this Hamiltonian are denoted as $|+\rangle_i = \alpha|g\rangle_i + \beta|e_+\rangle_i$ and $|-\rangle_i = -\beta|g\rangle_i + \alpha|e_+\rangle_i$ with energies $\pm\sqrt{\Delta^2 + \Omega^2}/2$.

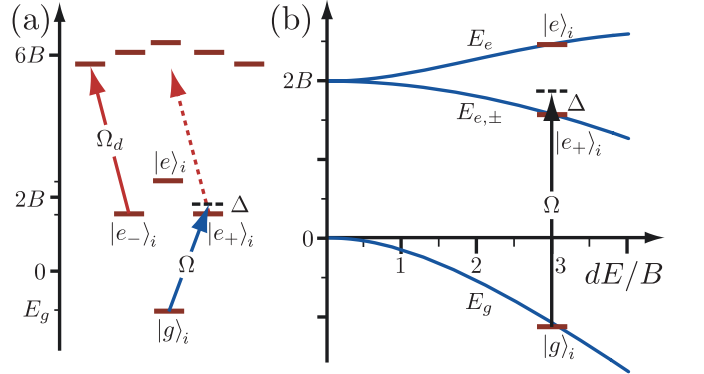


FIG. 13: Spectrum of a polar molecule. (a) Level structure for $Ed/B = 3$: the circular polarized microwave field couples the ground state $|g\rangle$ with the excited state $|e_+\rangle$ with Rabi frequency Ω/\hbar and detuning Δ . The excited state $|e_+\rangle$ is characterized by a finite angular momentum $J_z|e_+\rangle = |e_+\rangle$. Applying a second microwave field with opposite polarization (red arrow) allows us to lift the degeneracy in the first excited manifold by resonantly couple the state $|e_-\rangle$ to the next manifold. (b) Internal excitation energies for a single polar molecule in a static electric field $\mathbf{E} = E\mathbf{e}_z$.

For distances $|\mathbf{r}_{ij}| \gg (D/B)^{1/3}$ with $D = |\langle g|\mathbf{d}_i|e_+\rangle|^2$ and \mathbf{d}_i the dipole operator, the dipole-dipole interaction Eq. (4) between two polar molecules can be mapped onto the effective spin interaction Hamiltonian $H_d = H_d^{\text{int}} + H_d^{\text{shift}}$. The first term describes an effective spin-spin interaction

$$H_d^{\text{int}} = -\frac{1}{2} \sum_{i \neq j} D\nu(\mathbf{r}_{ij}) [S_i^x S_j^x + S_i^y S_j^y - \eta_{\pm}^2 S_i^z S_j^z], \quad (32)$$

where $\eta_{\pm} = \eta_g \pm \eta_e$ is determined by the induced dipole moments $\eta_g = \partial_E E_g / \sqrt{D}$ and $\eta_e = \partial_E E_{e,+} / \sqrt{D}$. The anisotropic behavior of the dipole-dipole interaction is accounted for by $\nu(\mathbf{r}) = (1 - 3\cos^2\vartheta)/r^3$ with ϑ the angle between \mathbf{r} and the z -axis. In addition, the asymmetry of the induced dipole moments gives rise to a position dependent renormalization of the effective magnetic field and a energy shift

$$H_d^{\text{shift}} = \frac{1}{2} \sum_{i \neq j} D\nu(\mathbf{r}_{ij}) \left[\frac{\eta_- \eta_+}{2} S_i^z + \frac{\eta_{\pm}^2}{4} \right]. \quad (33)$$

Within the Born-Oppenheimer approximation, an analytic expression for the effective interaction $V_{\text{eff}}(\{\mathbf{r}_i\})$ between two polar molecules each prepared in the state $|+\rangle_i$ can be derived in second-order perturbation theory in the dipole-dipole interaction $V_{\text{dd}}(\mathbf{r})/\hbar$ as

$$V_{\text{eff}}(\{\mathbf{r}_i\}) = E^{(1)}(\{\mathbf{r}_i\}) + E^{(2)}(\{\mathbf{r}_i\}) \quad (34)$$

where $D/(a^3|\mathbf{h}|) = (R_0/a)^3 \ll 1$ is the (small) parameter controlling the perturbative expansion, a is the characteristic length scale of the interparticle separation and $R_0 = (D/\sqrt{\Delta^2 + \Omega^2})^{1/3}$ is a Condon point, analogous to that discussed in Sect. III B 2. The energy shift

$$E^{(1)}(\{\mathbf{r}_i\}) = \frac{1}{2} \left[(\alpha^2 \eta_g + \beta^2 \eta_e)^2 - \alpha^2 \beta^2 \right] \sum_{i \neq j} D \nu(\mathbf{r}_{ij}), \quad (35)$$

gives rise to a dipole-dipole interaction between the particles, while the term

$$E^{(2)}(\{\mathbf{r}_i\}) = \sum_{k \neq i, k \neq j} \frac{|M|^2}{\sqrt{\Delta^2 + \Omega^2}} D^2 \nu(\mathbf{r}_{ik}) \nu(\mathbf{r}_{jk}) + \sum_{i < j} \frac{|N|^2}{2\sqrt{\Delta^2 + \Omega^2}} [D \nu(\mathbf{r}_{ij})]^2. \quad (36)$$

corresponds to a correction to the two-particle interaction potential and an additional three-body interaction. The matrix elements M and N take the form

$$M = \alpha \beta \left[(\alpha^2 \eta_g + \beta^2 \eta_e) (\eta_e - \eta_g) - (\alpha^2 - \beta^2)/2 \right], \\ N = \alpha^2 \beta^2 \left[(\eta_e - \eta_g)^2 + 1 \right].$$

Therefore, the effective interaction potential V_{eff} up to second order in $(R_0/a)^3$ reduces to the form in Eq. (2) with the two-particle interaction potential

$$V(\mathbf{r}) = \lambda_1 D \nu(\mathbf{r}) + \lambda_2 D R_0^3 [\nu(\mathbf{r})]^2, \quad (37)$$

and the three-body interaction

$$W(\mathbf{r}_1, \mathbf{r}_2, \mathbf{r}_3) = \gamma_2 R_0^3 D [\nu(\mathbf{r}_{12}) \nu(\mathbf{r}_{13}) + \nu(\mathbf{r}_{12}) \nu(\mathbf{r}_{23}) + \nu(\mathbf{r}_{13}) \nu(\mathbf{r}_{23})]. \quad (38)$$

The dimensionless coupling parameters are $\lambda_1 = (\alpha^2 \eta_g + \beta^2 \eta_e)^2 - \alpha^2 \beta^2$, $\lambda_2 = 2|M|^2 + |N|^2/2$, and $\gamma_2 = 2|M|^2$. These parameters can be tuned via the strength of the electric field Ed/B and the ratio between the Rabi frequency and the detuning, Ω/Δ , see Fig. 14. Of special interest are the values of the external fields where the leading two-particle interaction vanishes, i.e. $\lambda_1 = 0$. Then, the interaction is dominated by the second order contribution with λ_2 and γ_2 , which includes the three-body interaction, see Fig. 14(d), while a small deviation away from the line $\lambda_1 = 0$ allows us to change the character of the two-particle interaction. Note, that a n -body interaction term ($n \geq 4$) appears in $(n-1)$ -th order perturbation theory in the small parameter $(R_0/a)^3$. Therefore, the contribution of these terms is suppressed and can be safely ignored.

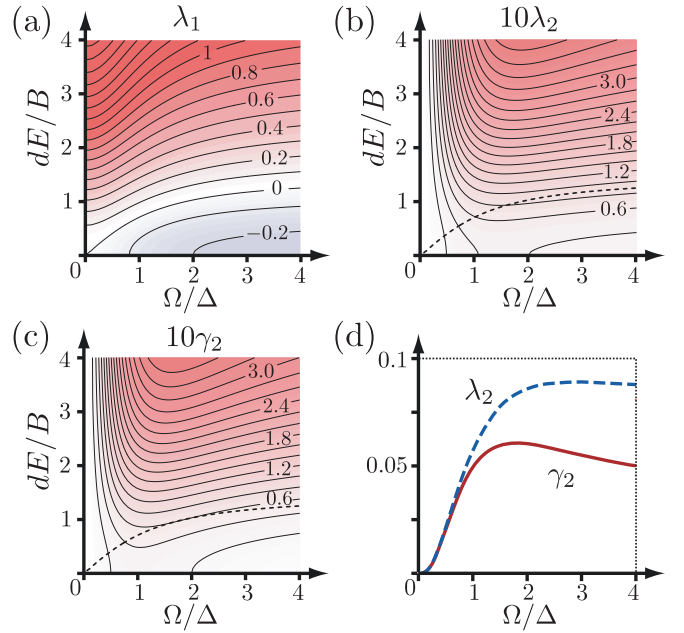


FIG. 14: Parameters of the effective interaction potential. (a)-(c): Strength of the interaction parameters λ_1 , λ_2 , and γ_2 as a function of the external fields Ed/B and Ω/Δ . The leading dipole-dipole interaction vanishes for $\lambda_1 = 0$ [dashed line in (b) and (c)], and the second order contributions dominate the interaction. (d) Strength of λ_2 (dashed line) and γ_2 (solid line) along the line in parameter space with $\lambda_1 = 0$.

The perturbative expansion requires that $a \gg R_0$. We notice that particles can be confined to interparticle distances larger than R_0 by combining *repulsive* dipole-dipole interactions with a strong (optical) transverse confinement ω_\perp , in analogy to Sect. III B 1. Then, for a repulsive two-particle potential with $\lambda_1 \gtrsim -\lambda_2(R_0/a)^3$ and for $\hbar\omega_\perp > D/R_0^3$, two-particles reach distances $|\mathbf{r}_i - \mathbf{r}_j| < R_0$ at an exponentially small rate $\Gamma \sim (\hbar/ma^2) \exp(-2S_E/\hbar)$, with $S_E/\hbar \sim \sqrt{Dm/R_0\hbar^2}$. This exponential suppression ensures the stability of the collisional setup for the duration of an experiment.

The low-energy many-body theory now follows by combining the kinetic energy of the polar molecules with the effective interaction V_{eff} within the Born-Oppenheimer approximation and the external trapping potentials V_T

$$H = \sum_i \frac{\mathbf{p}_i^2}{2m} + V_{\text{eff}}(\{\mathbf{r}_i\}) + \sum_i V_T(\mathbf{r}_i). \quad (39)$$

This Hamiltonian is independent of the statistics of the particles and therefore it is valid for bosonic and fermionic polar molecules.

Applying an optical lattice provides a periodic structure for the polar molecules described by the Hamiltonian Eq. (39). In the limit of a deep lattice, a standard expansion of the field operators $\psi^\dagger(\mathbf{r}) = \sum_i w(\mathbf{r} - \mathbf{R}_i) b_i^\dagger$ in the second-quantized expression of Eq. (39) in terms

of lowest-band Wannier functions $w(\mathbf{r})$ and particle creation operators b_i^\dagger ¹⁰⁷ leads to the realization of the Hubbard model of Eq. (9), characterized by strong nearest-neighbor interactions⁸⁹. We notice that the particles are treated as hard-core because of the constraint $a \gg R_0$. The interaction parameters U_{ij} and V_{ijk} in Eq. (9) derive from the effective interaction $V(\{\mathbf{r}_i\})$, and in the limit of well-localized Wannier functions reduce to

$$U_{ij} = U_0 \frac{a^3}{|\mathbf{R}_i - \mathbf{R}_j|^3} + U_1 \frac{a^6}{|\mathbf{R}_i - \mathbf{R}_j|^6}, \quad (40)$$

and

$$W_{ijk} = W_0 \left[\frac{a^6}{|\mathbf{R}_i - \mathbf{R}_j|^3 |\mathbf{R}_i - \mathbf{R}_k|^3} + perm \right], \quad (41)$$

respectively, with $U_0 = \lambda_1 D/a^3$, $U_1 = \lambda_2 DR_0^3/a^6$, and $W_0 = \gamma_2 DR_0^3/a^6$. The dominant contributions and strengths of the three-body terms in different lattice geometries are shown in Fig. 2(b). For LiCs with a permanent dipole moment $d = 6.3$ Debye trapped in an optical lattice with spacing $a \approx 500$ nm, the leading dipole-dipole interaction can give rise to very strong nearest-neighbor interactions with $U_0 \sim 55 E_{\text{kin}}$, and $E_{\text{kin}} = \hbar^2/ma^2$. On the other hand, tuning the parameters via the external fields to $\lambda_1 = 0$ the characteristic energy scale for the three-body interaction becomes $W_0 \approx (R_0/a)^3 E_{\text{kin}}$. Then, controlling the hopping energy J via the strength of the optical lattice allows to enter the regime with dominant three-body interactions. For particles been bosons, an analytic calculation has suggested that the ground-state phase diagram of Eq. (9) with $U_{ij} = 0$ in 1D is characterized by the presence of valence bond states at specific rational fillings of the lattice, charge-density waves and superfluid phases⁸⁹.

D. Lattice Spin models

Cold gases of polar molecules allow to construct in a natural way a *complete toolbox* for any permutation symmetric two spin-1/2 (qubit) interaction, using techniques of interaction engineering similar to those discussed in the previous sections.

The system we have in mind is comprised of heteronuclear molecules with $^2\Sigma_{1/2}$ ground electronic states, corresponding for example to alkaline-earth monohalogenides with a single electron outside a closed shell. We adopt a model molecule where the rotational excitations are described by the Hamiltonian

$$H_m = BN^2 + \gamma \mathbf{N} \cdot \mathbf{S}, \quad (42)$$

with \mathbf{N} the dimensionless orbital angular momentum of the nuclei, and \mathbf{S} the dimensionless electronic spin (assumed to be $S = 1/2$ in the following). Here B denotes the rotational constant and γ is the spin-rotation coupling constant, where a typical B is a few tens of GHz,

and γ in the hundred MHz regime. The coupled basis of a single molecule i corresponding to the eigenbasis of H_m^i is $\{|N_i, S_i, J_i; M_{J_i}\rangle\}$ where $\mathbf{J}_i = \mathbf{N}_i + \mathbf{S}_i$ with eigenvalues $E(N = 0, 1/2, 1/2) = 0$, $E(1, 1/2, 1/2) = 2B - \gamma$, and $E(1, 1/2, 3/2) = 2B + \gamma/2$.

The Hamiltonian describing the internal and external dynamics of a pair of molecules trapped in wells of an optical lattice is denoted by $H = H_{\text{in}} + H_{\text{ex}}$. The interaction describing the internal degrees of freedom is $H_{\text{in}} = H_{\text{dd}} + \sum_{i=1}^2 H_m^i$, where H_{dd} is the dipole-dipole interaction. The Hamiltonian describing the external, or motional, degrees of freedom is $H_{\text{ex}} = \sum_{i=1}^2 \mathbf{P}_i^2/(2m) + V_i(\mathbf{x}_i - \bar{\mathbf{x}}_i)$, where \mathbf{P}_i is the momentum of molecule i with mass m , and the potential generated by the optical lattice $V_i(\mathbf{x} - \bar{\mathbf{x}}_i)$ describes an external confinement of molecule i about a local minimum $\bar{\mathbf{x}}_i$ with 1D rms width z_0 . We assume isotropic traps that are approximately harmonic near the trap minimum with a vibrational spacing $\hbar\omega_{\text{osc}}$. Furthermore, we assume that the molecules can be prepared in the motional ground state of each local potential using dissipative electromagnetic pumping¹³². It is convenient to define the quantization axis \hat{z} along the axis connecting the two molecules, $\bar{\mathbf{x}}_2 - \bar{\mathbf{x}}_1 = \Delta z \hat{z}$ with Δz corresponding to a multiple of the lattice spacing.

The ground subspace of each molecule is isomorphic to a spin 1/2 particle. Our goal is to obtain an effective spin-spin interaction between two neighboring molecules. Static spin-spin interactions due to spin-rotation and dipole-dipole couplings do exist but are very small in our model: $H_{\text{vdW}}(r) = -(d^4/2Br^6) \left[1 + (\gamma/4B)^2 (1 + 4\mathbf{S}_1 \cdot \mathbf{S}_2/3 - 2S_1^z S_2^z) \right]$. The first term is the familiar van-der-Waals $1/r^6$ interaction, while the spin dependent piece is strongly suppressed as $\gamma/4B \approx 10^{-3} \ll 1$. However, dipole-dipole coupled excited states can be dynamically mixed using a microwave field.

The molecules are assumed to be trapped with a separation $\Delta z \sim r_\gamma \equiv (2d^2/\gamma)^{1/3}$, where the dipole dipole interaction is $d^2/r_\gamma^3 = \gamma/2$. In this regime the rotation of the molecules is strongly coupled to the spin and the excited states are described by Hund's case (c) states in analogy to the dipole-dipole coupled excited electronic states of two atoms with fine-structure. The ground states are essentially spin independent. In the subspace of one rotational quantum ($N_1 + N_2 = 1$), there are 24 eigenstates of H_{in} which are linear superpositions of two electron spin states and properly symmetrized rotational states of the two molecules. There are several symmetries that reduce H_{in} to block diagonal form. First, H_{dd} , conserves the quantum number $Y = M_N + M_S$ where $M_N = M_{N_1} + M_{N_2}$ and $M_S = M_{S_1} + M_{S_2}$ are the total rotational and spin projections along the intermolecular axis. Second, parity, defined as the interchange of the two molecules followed by parity through the center of each molecule, is conserved. The $\sigma = \pm 1$ eigenvalues of parity are conventionally denoted $g(u)$ for *gerade(ungerade)*. Finally, there is a symme-

try associated with reflection R of all electronic and rotational coordinates through a plane containing the intermolecular axis. For $|Y| > 0$ all eigenstates are even under R but for states with zero angular momentum projection there are ± 1 eigenstates of R . The 16 distinct eigenvalues correspond to degenerate subspaces labeled $|Y|_{\sigma}^{\pm}(J)$ with J indicating the quantum number in the $r \rightarrow \infty$ asymptotic manifold ($N = 0, J = 1/2; N = 1, J$). Remarkably, the eigenvalues and eigenstates can be computed analytically yielding the Movre-Pichler potentials¹³³ plotted in Fig. 15(a).

In order to induce strong dipole-dipole coupling we introduce a microwave field $E(\mathbf{x}, t)\mathbf{e}_F$ with a frequency ω_F and Rabi-frequency Ω tuned near resonance with the $N = 0 \rightarrow N = 1$ transition.

The effective Hamiltonian acting on the lowest-energy states is obtained in second order perturbation theory as

$$H_{\text{eff}}(r) = \sum_{i,f} \sum_{\lambda(r)} \frac{\langle g_f | H_{\text{mf}} | \lambda(r) \rangle \langle \lambda(r) | H_{\text{mf}} | g_i \rangle}{\hbar\omega_F - E(\lambda(r))} |g_f\rangle \langle g_i|, \quad (43)$$

where $\{|g_i\rangle, |g_f\rangle\}$ are ground states with $N_1 = N_2 = 0$ and $\{|\lambda(r)\rangle\}$ are excited eigenstates of H_{in} with $N_1 + N_2 = 1$ and with excitation energies $\{E(\lambda(r))\}$. The reduced interaction in the subspace of the spin degrees of freedom is then obtained by tracing over the motional degrees of freedom. For molecules trapped in the ground motional states of isotropic harmonic wells with rms width z_0 the wave function is separable in center of mass and relative coordinates, and the effective spin-spin Hamiltonian is $H_{\text{spin}} = \langle H_{\text{eff}}(r) \rangle_{\text{rel}}$.

The Hamiltonian in Eq. (43) is guaranteed to yield some entangling interaction for appropriate choice of field parameters but it is desirable to have a systematic way to design a spin-spin interaction. The model presented here possesses sufficient structure to achieve this essentially analytically. The effective Hamiltonian on molecules 1 and 2 induced by a microwave field is

$$H_{\text{eff}}(r) = \frac{\hbar|\Omega|}{8} \sum_{\alpha,\beta=0}^3 \sigma_1^{\alpha} A_{\alpha,\beta}(r) \sigma_2^{\beta}, \quad (44)$$

where $\{\sigma^{\alpha}\}_{\alpha=0}^3 \equiv \{\mathbf{1}, \sigma^x, \sigma^y, \sigma^z\}$ and A is a real symmetric tensor.

Equation (44) describes a generic permutation symmetric two qubit Hamiltonian. The components $A_{0,s}$ describe a pseudo magnetic field which acts locally on each spin and the components $A_{s,t}$ describe two qubit coupling. The pseudo magnetic field is zero if the microwave field is linearly polarized but a real magnetic field could be used to tune local interactions and, given a large enough gradient, could break the permutation invariance of H_{spin} .

For a given field polarization, tuning the frequency near an excited state induces a particular spin pattern on the ground states. These patterns change as the frequency is tuned though multiple resonances at a fixed

TABLE I: Some spin patterns that result from Eq. (44). The field polarization is given with respect to the intermolecular axis \hat{z} and the frequency ω_F is chosen to be near resonant with the indicated excited state potential at the internuclear separation Δz . The sign of the interaction will depend on whether the frequency is tuned above or below resonance.

Polarization	Resonance	Spin pattern
\hat{x}	2_g	$\sigma^z \sigma^z$
\hat{z}	0_u^+	$\vec{\sigma} \cdot \vec{\sigma}$
\hat{z}	0_g^-	$\sigma^x \sigma^x + \sigma^y \sigma^y - \sigma^z \sigma^z$
\hat{y}	0_g^-	$\sigma^x \sigma^x - \sigma^y \sigma^y + \sigma^z \sigma^z$
\hat{y}	0_g^+	$-\sigma^x \sigma^x + \sigma^y \sigma^y + \sigma^z \sigma^z$
$(\hat{y} - \hat{x})/\sqrt{2}$	0_g^+	$-\sigma^x \sigma^y - \sigma^y \sigma^x + \sigma^z \sigma^z$
$\cos \xi \hat{x} + \sin \xi \hat{z}$	1_g	$\lambda_1(\sigma^x \sigma^z + \sigma^z \sigma^x) + \lambda_2 \sigma^z \sigma^z + \lambda_3(\sigma^x \sigma^x + \sigma^y \sigma^y)$
$\cos \xi \hat{y} + \sin \xi \hat{z}$	1_g	$\lambda_1(\sigma^y \sigma^z + \sigma^z \sigma^y) + \lambda_2 \sigma^z \sigma^z + \lambda_3(\sigma^x \sigma^x + \sigma^y \sigma^y)$

intermolecular separation. In Table I it is shown how to simulate the Ising and Heisenberg interactions in this way. Using several fields that are sufficiently separated in frequency, the resulting effective interactions are additive creating a *spin texture* on the ground states. The anisotropic spin model $H_{XYZ} = \lambda_x \sigma^x \sigma^x + \lambda_y \sigma^y \sigma^y + \lambda_z \sigma^z \sigma^z$ can be simulated using three fields: one polarized along \hat{z} tuned to $0_u^+(3/2)$, one polarized along \hat{y} tuned to $0_g^-(3/2)$ and one polarized along \hat{y} tuned to $0_g^+(1/2)$. The strengths λ_j can be tuned by adjusting the Rabi frequencies and detunings of the three fields. Using an external magnetic field and six microwave fields with, for example, frequencies and polarizations corresponding to the last six spin patterns in Table I, arbitrary permutation symmetric two qubit interaction are possible.

The Kitaev model of Eq. (11) (Spin model II) can be obtained in the following way. Consider a system of four molecules connected by three length b edges forming an orthogonal triad in space. There are several different microwave field configurations that can be used to realize the interaction $H_{\text{spin}}^{(\text{II})}$ along the links. One choice is to use two microwave fields polarized along \hat{z} , one tuned near resonance with a 1_g potential and one near a 1_u potential. A realization of model II using a different set of 3 microwave fields is shown in Fig. 15(b). The obtained interaction is close to ideal with small residual coupling to next nearest neighbors.

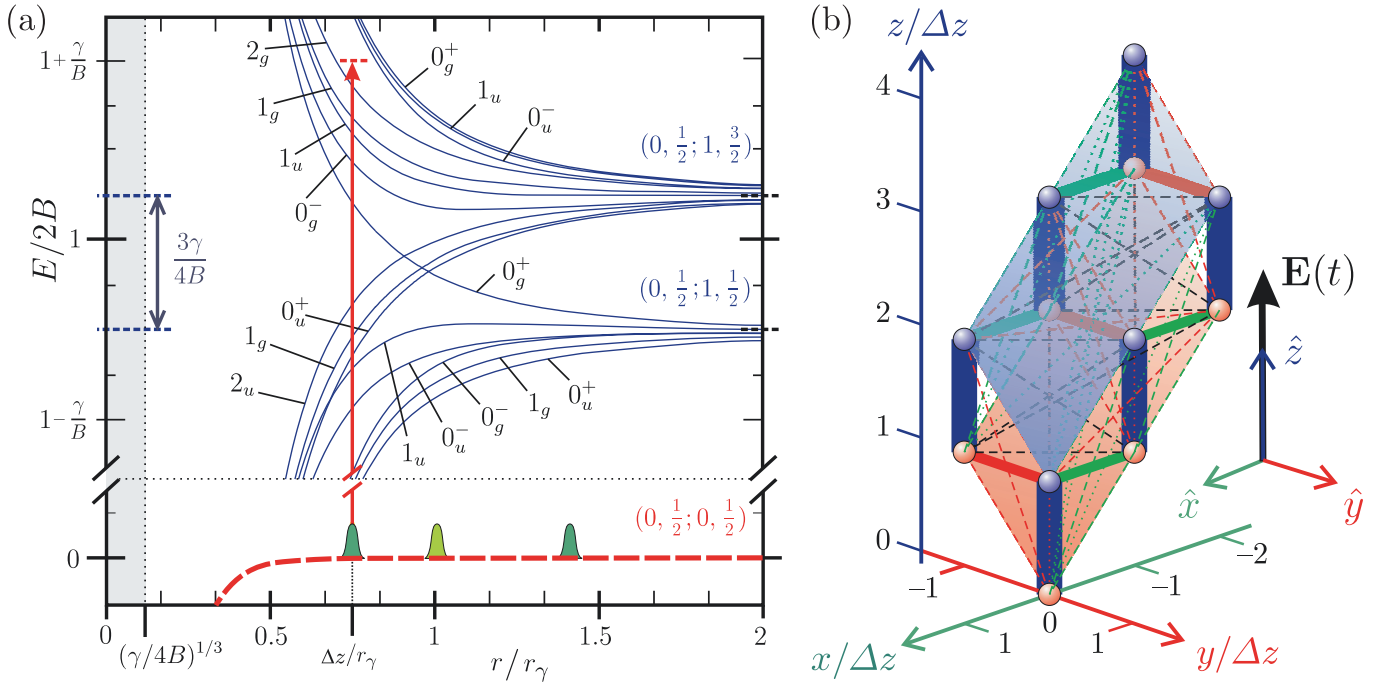


FIG. 15: (a) Movre-Pichler potentials for a pair of molecules as a function of their separation r : The potentials $E(g_i(r))$ for the 4 ground-state (dashed lines) and the potentials $E(\lambda(r))$ for the first 24 excited states (solid lines). The symmetries $|Y_{\sigma}^{\pm}|$ of the corresponding excited manifolds are indicated, as are the asymptotic manifolds $(N_i, J_i; N_j, J_j)$. (b) Implementation of spin model $H_{\text{spin}}^{(\text{II})}$. Shown is the spatial configuration of 12 polar molecules trapped by two parallel triangular lattices (indicated by shaded planes) with separation normal to the plane of $\Delta z/\sqrt{3}$ and in plane relative lattice shift of $\Delta z\sqrt{2/3}$. Nearest neighbors are separated by $b = \Delta z$ and next nearest neighbor couplings are at $\sqrt{2}b$. The graph vertices represent spins and the edges correspond to pairwise spin couplings. The edge color indicates the nature of the dominant pairwise coupling for that edge (blue = $\sigma^z\sigma^z$, red = $\sigma^y\sigma^y$, green = $\sigma^x\sigma^x$, black = “other”). For nearest neighbor couplings, the edge width indicates the relative strength of the absolute value of the coupling. For this implementation, the nearest neighbor separation is $b = r_{\gamma}$. Three fields all polarized along \hat{z} were used to generate the effective spin-spin interaction with frequencies and intensities optimized to approximate the ideal model $H_{\text{spin}}^{(\text{II})}$. The field detunings at the nearest neighbor spacing are: $\hbar\omega_1 - E(1_g(1/2)) = -0.05\gamma/2$, $\hbar\omega_2 - E(0_g^-(1/2)) = 0.05\gamma/2$, $\hbar\omega_3 - E(2_g(3/2)) = 0.10\gamma/2$ and the amplitudes are $|\Omega_1| = 4|\Omega_2| = |\Omega_3| = 0.01\gamma/\hbar$. For $\gamma = 40\text{MHz}$ this generates effective coupling strengths $J_z = -100\text{kHz}$ and $J_{\perp} = -0.4J_z$. The magnitude of residual nearest neighbor couplings are less than $0.04|J_z|$ along x and y -links and less than $0.003|J_z|$ along z -links. The size of longer range couplings J_{lr} are indicated by edge line style (dashed: $|J_{\text{lr}}| < 0.01|J_z|$, dotted: $|J_{\text{lr}}| < 10^{-3}|J_z|$). Treating pairs of spins on z -links as a single effective spin in the low energy sector, the model approximates Kitaev’s 4-local Hamiltonian¹¹⁵ on a square grid (shown here are one plaquette on the square lattice and a neighbor plaquette on the dual lattice) with an effective coupling strength $J_{\text{eff}} = -(J_{\perp}/J_z)^4|J_z|/16 \approx 167\text{Hz}$.

¹ For an overview, see e.g. *Ultracold matter*, Nature Insight, Nature (London) **416**, 205246 (2002).

² See e.g. *Special Issue: Ultracold Polar Molecules: Formation and Collisions*, Eur. Phys. J. D **31**, 149-445 (2004).

³ J. M. Sage, S. Sainis, T. Bergeman, and D. DeMille, *Optical Production of Ultracold Polar Molecules*, Phys. Rev. Lett. **94**, 203001 (2005).

⁴ H. L. Bethlem, G. Berden, F. M. H. Crompvoets, R. T. Jongma, A. J. A. van Roij and G. Meijer, *Electrostatic trapping of ammonia molecules*, Nature (London) **406**, 491 (2000).

⁵ J. D. Weinstein, R. deCarvalho, T. Guillet, B. Friedrich and J. M. Doyle, *Magnetic trapping of calcium monohy-*

dride molecules at millikelvin temperatures, Nature **395**, 148 (1998).

⁶ F. M.H. Crompvoets, H. L. Bethlem, R. T. Jongma and G. Meijer, *A prototype storage ring for neutral molecules*, Nature (London) **411**, 174 (2001).

⁷ T. Junglen, T. Rieger, S. A. Rangwala, P.W. H. Pinkse, and G. Rempe, *Two-Dimensional Trapping of Dipolar Molecules in Time-Varying Electric Fields*, Phys. Rev. Lett. **92**, 223001 (2004).

⁸ M. R. Tarbutt, H. L. Bethlem, J. J. Hudson, V. L. Ryabov, V. A. Ryzhov, B. E. Sauer, G. Meijer, and E. A. Hinds, *Slowing Heavy, Ground-State Molecules using an Alternating Gradient Decelerator*, Phys. Rev. Lett. **92**,

- 173002 (2004).
- ⁹ T. Rieger, T. Junglen, S. A. Rangwala, P. W. H. Pinkse, and G. Rempe, *Continuous Loading of an Electrostatic Trap for Polar Molecules*, Phys. Rev. Lett. **95**, 173002 (2005).
 - ¹⁰ D. Wang, J. Qi, M. F. Stone, O. Nikolayeva, H. Wang, B. Hattaway, S. D. Gensemer, P. L. Gould, E. E. Eyler, and W. C. Stwalley, *Photoassociative Production and Trapping of Ultracold KRb Molecules*, Phys. Rev. Lett. **93**, 243005 (2004).
 - ¹¹ S. Y. T. van de Meerakker, P. H. M. Smeets, N. Vanhaecke, R. T. Jongma, and G. Meijer *Deceleration and Electrostatic Trapping of OH Radicals*, Phys. Rev. Lett. **94**, 023004 (2005).
 - ¹² S. D. Kraft, P. Staunum, J. Lange, L. Vogel, R. Wester, and M. Weidemüller, *Formation of ultracold LiCs molecules*, J. Phys. B **39**, S993 (2006).
 - ¹³ S. Ospelkaus, A. Pe'er, K.-K. Ni, J. J. Zirbel, B. Neyenhuis, S. Kotochigova, P. S. Julienne, J. Ye, and D. S. Jin, *Ultracold dense gas of deeply bound heteronuclear molecules*, arXiv:0802.1093
 - ¹⁴ S. Knoop, M. Mark, F. Ferlaino, J.G. Danzl, T. Kraemer, H.-C. Naegerl, and R. Grimm, *Metastable Feshbach Molecules in High Rotational States*, Phys. Rev. Lett. **100**, 083002 (2008).
 - ¹⁵ F. Lang, P. v. d. Straten, B. Brandstätter, G. Thalhammer, K. Winkler, P. S. Julienne, R. Grimm, and J. Hecker Denschlag, *Cruising through molecular bound-state manifolds with radiofrequency*, Nature Physics **4**, 223 (2008).
 - ¹⁶ B. C. Sawyer, B. L. Lev, E. R. Hudson, B. K. Stuhl, M. Lara, J. L. Bohn, Jun Ye, *Magneto-electrostatic trapping of ground state OH molecules*, Phys. Rev. Lett. **98**, 253002 (2007).
 - ¹⁷ W.C. Stwalley, *Efficient conversion of ultracold Feshbach-resonance-related polar molecules into ultracold ground state ($X^1\Sigma^+v = 0, J = 0$) molecules*, Eur. Phys. J. D **31**, 221 (2004)
 - ¹⁸ E.R. Hudson, J.R. Bochinski, H.J. Lewandowski, B.C. Sawyer, and J.Ye, *Efficient Stark deceleration of cold polar molecules*, Eur. Phys. J. D **31**, 351 (2004)
 - ¹⁹ S. Inouye, J. Goldwin, M. L. Olsen, C. Ticknor, J. L. Bohn, and D. S. Jin, *Observation of Heteronuclear Feshbach Resonances in a Mixture of Bosons and Fermions*, Phys. Rev. Lett. **93**, 183201 (2004)
 - ²⁰ D. DeMille, *Quantum Computation with Trapped Polar Molecules*, Phys. Rev. Lett. **88**, 067901 (2002).
 - ²¹ M. Greiner, C. A. Regal, and D. S. Jin, *Emergence of a molecular Bose-Einstein condensate from a Fermi gas*, Nature (London) **426**, 537-540 (2003).
 - ²² C. A. Regal, C. Ticknor, J. L. Bohn, and D. S. Jin, *Creation of ultracold molecules from a Fermi gas of atoms*, Nature (London) **424**, 47 (2003).
 - ²³ T. Volz, N. Syassen, D. M. Bauer, E. Hansis, S. Dürr and G. Rempe, *Preparation of a quantum state with one molecule at each site of an optical lattice*, Nature Physics **2**, 692 (2006).
 - ²⁴ U. Fano, *Effects of Configuration Interaction on Intensities and Phase Shifts*, Phys. Rev. **124**, 1866 (1961); U. Fano, *Sullo spettro di assorbimento dei gas nobili presso il limite dello spettro d'arco*, Nuovo Cimento **12**, 154 (1935) [in English at: U. Fano, G. Pupillo, A. Zannoni, and C. W. Clark, *On the absorption spectrum of noble gases at the arc spectrum limit*, J. Res. Natl. Inst. Stand. Technol. **110**, 583 (2005)].
 - ²⁵ For a review on Feshbach resonances see e.g. R. A. Duine and H. T. C. Stoof, *Atom molecule coherence in Bose gases*, Phys. Rep. **396**, 115 (2004).
 - ²⁶ C. A. Regal, M. Greiner, and D. S. Jin, *Observation of Resonance Condensation of Fermionic Atom Pairs*, Phys. Rev. Lett. **92**, 040403 (2004).
 - ²⁷ M. Bartenstein, A. Altmeyer, S. Riedl, S. Jochim, C. Chin, J. Hecker Denschlag, and R. Grimm, *Crossover from a Molecular Bose-Einstein Condensate to a Degenerate Fermi Gas*, Phys. Rev. Lett. **92**, 120401 (2004).
 - ²⁸ M. W. Zwierlein, J. R. Abo-Shaeer, A. Schirotzek, C. H. Schunck and W. Ketterle, *Vortices and superfluidity in a strongly interacting Fermi gas*, Nature (London) **435**, 1047 (2005).
 - ²⁹ G. B. Partridge, K. E. Strecker, R. I. Kamar, M. W. Jack, and R. G. Hulet, *Molecular Probe of Pairing in the BEC-BCS Crossover*, Phys. Rev. Lett. **95**, 020404 (2005).
 - ³⁰ C. Chin, M. Bartenstein, A. Altmeyer, S. Riedl, S. Jochim, J. Hecker Denschlag, and R. Grimm, *Observation of the Pairing Gap in a Strongly Interacting Fermi Gas*, Science **305**, 1128 (2005).
 - ³¹ Z. Hadzibabic, P. Krüger, M. Cheneau, B. Battelier, J. B. Dalibard, *Berezinskii-Kosterlitz-Thouless Crossover in a Trapped Atomic Gas*, Nature **441**, 1118 (2006).
 - ³² M. Greiner, O. Mandel, T. Esslinger, T.W. Hänsch, and I. Bloch, *Quantum Phase Transition from a Superfluid to a Mott Insulator in a Gas of Ultracold Atoms*, Nature (London) **415**, 39 (2002).
 - ³³ I. B. Spielman, W. D. Phillips, and J. V. Porto, *Mott-Insulator Transition in a Two-Dimensional Atomic Bose Gas*, Phys. Rev. Lett. **98**, 080404 (2007).
 - ³⁴ T. Koch, T. Lahaye, J. Metz, B. Frhlich, A. Griesmaier, and T. Pfau, *Stabilizing a purely dipolar quantum gas against collapse*, Nature Physics **4**, 218 (2008).
 - ³⁵ T. Lahaye, T. Koch, B. Froehlich, M. Fattori, J. Metz, A. Griesmaier, S. Giovanazzi, and T. Pfau, *Strong dipolar effects in a quantum ferrofluid*, Nature **448**, 672 (2007).
 - ³⁶ A. Griesmaier, J. Stuhler, T. Koch, M. Fattori, T. Pfau, and S. Giovanazzi, *Comparing contact and dipolar interaction in a Bose-Einstein condensate*, Phys. Rev. Lett. **97**, 250402 (2006).
 - ³⁷ See the up-coming review: M A. Baranov, *Theoretical progress in many-body physics with ultracold dipolar gases*, Phys. Rep., in press, and references therein.
 - ³⁸ D.-W. Wang, M. D. Lukin, and E. Demler, *Quantum Fluids of Self-Assembled Chains of Polar Molecules*, Phys. Rev. Lett. **97**, 180413 (2006)
 - ³⁹ D.-W. Wang, *Quantum phase transitions of polar molecules in bilayer systems*, Phys. Rev. Lett. **98**, 060403 (2007).
 - ⁴⁰ L. Santos, G.V. Shlyapnikov, P. Zoller, and M. Lewenstein, *Bose-Einstein Condensation in Trapped Dipolar Gases*, Phys. Rev. Lett. **85**, 1791 (2000).
 - ⁴¹ D. S. Petrov, G. E. Astrakharchik, D. J. Papoular, C. Salomon, and G. V. Shlyapnikov, *Crystalline Phase of Strongly Interacting Fermi Mixtures*, Phys. Rev. Lett. **99**, 130407 (2007).
 - ⁴² P. Pedri, S. De Palo, E. Orignac, R. Citro, and M. L. Chiofalo, *Collective excitations of trapped one-dimensional dipolar quantum gases*, Phys. Rev. A **77**, 015601 (2008).
 - ⁴³ C. Lee and E. A. Ostrovskaya, *Quantum computation with diatomic bits in optical lattices*, Phys. Rev. A **72**, 062321 (2005).
 - ⁴⁴ S. Kotochigova and E. Tiesinga, *Controlling polar*

- molecules in optical lattices*, Phys. Rev. A **73**, 041405(R) (2006).
- ⁴⁵ S. F. Yelin, K. Kirby, and R. Côté, *Schemes for robust quantum computation with polar molecules*, Phys. Rev. A **74**, 050301(R) (2006).
- ⁴⁶ E. Charron, P. Milman, A. Keller, and O. Atabek, *Quantum phase gate and controlled entanglement with polar molecules*, Phys. Rev. A **75**, 033414 (2007).
- ⁴⁷ S. Kotochigova, *Prospects for Making Polar Molecules with Microwave Fields*, Phys. Rev. Lett. **99**, 073003 (2007).
- ⁴⁸ D. DeMille, *Quantum Computation with Trapped Polar Molecules*, Phys. Rev. Lett. **88**, 067901 (2002).
- ⁴⁹ P. Rabl, D. DeMille, J. M. Doyle, M.D. Lukin, R.J. Schoelkopf, and P. Zoller, *Hybrid Quantum Processors: Molecular Ensembles as Quantum Memory for Solid State Circuits*, Phys. Rev. Lett. **97**, 033003 (2006).
- ⁵⁰ H. P. Büchler, E. Demler, M. D. Lukin, A. Micheli, N. V. Prokof'ev, G. Pupillo, and P. Zoller, *Strongly Correlated 2D Quantum Phases with Cold Polar Molecules: Controlling the Shape of the Interaction Potential*, Phys. Rev. Lett. **98**, 060404 (2007).
- ⁵¹ G. E. Astrakharchik, J. Boronat, I. L. Kurbakov, and Yu. E. Lozovik, *Quantum Phase Transition in a Two-Dimensional System of Dipoles*, Phys. Rev. Lett. **98**, 060405 (2007).
- ⁵² C. Mora, O. Parcollet, and X. Waintal, *Quantum melting of a crystal of dipolar bosons*, Phys. Rev. B **76**, 064511 (2007).
- ⁵³ A. S. Arkipov, G. E. Astrakharchik, A. V. Belikov, Yu. E. Lozovik, *Ground-state properties of a one-dimensional system of dipoles*, JETP **82**, 41 (2005).
- ⁵⁴ R. Citro, E. Orignac, S. De Palo, and M. L. Chiofalo, *Evidence of Luttinger-liquid behavior in one-dimensional dipolar quantum gases*, Phys. Rev. A **75**, 051602(R) (2007).
- ⁵⁵ P. Rabl and P. Zoller, *Molecular dipolar crystals as high-fidelity quantum memory for hybrid quantum computing*, Phys. Rev. A **76**, 042308 (2007).
- ⁵⁶ A. Micheli, G. K. Brennen, and P. Zoller, *A toolbox for lattice-spin models with polar molecules*, Nature Physics **2**, 341 (2006).
- ⁵⁷ G. K. Brennen, A. Micheli, and P. Zoller, *Designing spin-1 lattice models using polar molecules*, New J. Phys. **9**, 138 (2007).
- ⁵⁸ G. Pupillo, A. Griessner, A. Micheli, M. Ortner, D.-W. Wang, and P. Zoller, *Cold Atoms and Molecules in Self-Assembled Dipolar Lattices*, Phys. Rev. Lett. **100**, 050402 (2008).
- ⁵⁹ For studies in condensed matter setups see e.g.: D. Snoke, *Spontaneous Bose Coherence of Excitons and Polaritons*, Science **298**, 1368 (2002); S. De Palo, F. Rapisarda, and G. Senatore, *Excitonic Condensation in a Symmetric Electron-Hole Bilayer* Phys. Rev. Lett. **88**, 206401 (2002); D. V. Kulakovskii, Yu. E. Lozovik, and A. V. Chaplik, *Collective excitations in exciton crystal*, JETP **99**, 850 (2004), and references therein.
- ⁶⁰ B. Deb and L. You, *Low-energy atomic collision with dipole interactions*, Phys. Rev. A **64** (2001) 022717.
- ⁶¹ A. V. Avdeenkov and J. L. Bohn, *Linking Ultracold Polar Molecules*, Phys. Rev. Lett. **90**, 043006 (2003).
- ⁶² R. V. Krems, *Molecules near absolute zero and external field control of atomic and molecular dynamics*, Int. Rev. Phys. Chem. **24**, 99 (2005).
- ⁶³ R. V. Krems, *Controlling Collisions of Ultracold Atoms with dc Electric Fields*, Phys. Rev. Lett. **96**, 123202 (2006).
- ⁶⁴ C. Ticknor and J. Bohn, *Long-range scattering resonances in strong-field-seeking states of polar molecules*, Phys. Rev. A **72**, 032717 (2005).
- ⁶⁵ A. Derevianko, *Anisotropic pseudopotential for polarized dilute quantum gases*, Phys. Rev. A **67** (2003) 033607; A. Derevianko, *Erratum: Anisotropic pseudopotential for polarized dilute quantum gases*, [Phys. Rev. A **67** (2003) 033607] Phys. Rev. A **72** (2005) 03990.
- ⁶⁶ A. Micheli, G. Pupillo, H. P. Büchler, and P. Zoller, *Cold polar molecules in two-dimensional traps: Tailoring interactions with external fields for novel quantum phases*, Phys. Rev. A **76**, 043604 (2007).
- ⁶⁷ L. Santos, G. V. Shlyapnikov, and M. Lewenstein, *Roton-Maxon Spectrum and Stability of Trapped Dipolar Bose-Einstein Condensates*, Phys. Rev. Lett. **90**, 250403 (2003).
- ⁶⁸ D. H. O'Dell, S. Giovanazzi, and G. Kurizki, *Rotons in Gaseous Bose-Einstein Condensates Irradiated by a Laser*, Phys. Rev. Lett. **90**, 110402 (2003).
- ⁶⁹ D.C.E. Bortolotti, S. Ronen, J.L. Bohn, and D. Blume, *Scattering Length Instability in Dipolar Bose-Einstein Condensates*, Phys. Rev. Lett. **97** (2006) 160402.
- ⁷⁰ S. Ronen, D.C.E. Bortolotti, D. Blume, and J.L. Bohn, *Dipolar Bose-Einstein condensates with dipole-dependent scattering length*, Phys. Rev. A **74** (2006) 033611.
- ⁷¹ U. R. Fischer, *Stability of quasi-two-dimensional Bose-Einstein condensates with dominant dipole-dipole interactions*, Phys. Rev. A **73**, 031602(R) (2006).
- ⁷² S. Ronen, D.C.E. Bortolotti, and J.L. Bohn, *Radial and Angular Rotons in Trapped Dipolar Gases*, Phys. Rev. Lett. **98** (2007) 030406.
- ⁷³ P.M. Lushnikov, *Collapse of Bose-Einstein condensates with dipole-dipole interactions*, Phys. Rev. A **66** (2002) 051601(R)
- ⁷⁴ O. Dutta and P. Meystre, *Ground-state structure and stability of dipolar condensates in anisotropic traps*, Phys. Rev. A **75** (2007) 053604.
- ⁷⁵ S. Yi and L. You, *Trapped condensates of atoms with dipole interactions*, Phys. Rev. A **63** (2001) 053607.
- ⁷⁶ M. A. Baranov, K. Osterloh, and M. Lewenstein, *Fractional Quantum Hall States in Ultracold Rapidly Rotating Dipolar Fermi Gases*, Phys. Rev. Lett. **94**, 070404 (2005).
- ⁷⁷ D. H. O'Dell and C. Eberlein, *Vortex in a trapped Bose-Einstein condensate with dipole-dipole interactions*, Phys. Rev. A **75**, 013604 (2007).
- ⁷⁸ N. R. Cooper, E. H. Rezayi, and S. H. Simon, *Vortex Lattices in Rotating Atomic Bose Gases with Dipolar Interactions*, Phys. Rev. Lett. **95** (2005) 200402.
- ⁷⁹ J. Zhang and H. Zhai, *Vortex Lattices in Planar Bose-Einstein Condensates with Dipolar Interactions*, Phys. Rev. Lett. **95** (2005) 200403.
- ⁸⁰ S. Yi and H. Pu, *Vortex structures in dipolar condensates*, Phys. Rev. A **73** (2006) 061602(R).
- ⁸¹ K. Osterloh, N. Barberán, and M. Lewenstein, *Strongly Correlated States of Ultracold Rotating Dipolar Fermi Gases*, Phys. Rev. Lett. **99**, 160403 (2007).
- ⁸² K. Góral, L. Santos, and M. Lewenstein, *Quantum Phases of Dipolar Bosons in Optical Lattices*, Phys. Rev. Lett. **88**, 170406 (2002).
- ⁸³ R. Barnett, D. Petrov, M. Lukin, and E. Demler, *Quantum Magnetism with Multicomponent Dipolar Molecules*

- in an Optical Lattice, Phys. Rev. Lett. **96**, 190401 (2006).
- ⁸⁴ C. Menotti, C. Trefzger, and M. Lewenstein, *Metastable States of a Gas of Dipolar Bosons in a 2D Optical Lattice*, Phys. Rev. Lett. **98**, 235301 (2007).
- ⁸⁵ C. Kollath, J. S. Meyer, and T. Giamarchi, *Dipolar Bosons in a Planar Array of One-Dimensional Tubes*, Phys. Rev. Lett. **100**, 130403 (2008).
- ⁸⁶ E. G. Dalla Torre, E. Berg, and E. Altman, *Hidden Order in 1D Bose Insulators*, Phys. Rev. Lett. **97**, 260401 (2006).
- ⁸⁷ P. Sengupta, L. P. Pryadko, F. Alet, M. Troyer, and G. Schmid, *Supersolids versus Phase Separation in Two-Dimensional Lattice Bosons*, Phys. Rev. Lett. **94**, 207202 (2005).
- ⁸⁸ M. Boninsegni and N. Prokof'ev *Supersolid Phase of Hard-Core Bosons on a Triangular Lattice*, Phys. Rev. Lett. **95**, 237204 (2005).
- ⁸⁹ H.P. Büchler, A. Micheli and P. Zoller, *Three-body interactions with cold polar molecules*, Nature Physics **3**, 726 (2007).
- ⁹⁰ For oscillating time-dependent electric fields with frequency ω we transform H_{BO} by Fourier expansion in ω to a Floquet picture, and thus a time-independent Hamiltonian, whose eigenvalues provide the dressed Born-Oppenheimer potentials.
- ⁹¹ D.J. Wineland, C. Monroe, W.M. Itano, D. Leibfried, B.E. King, and D.M. Meekhof, *Experimental issues in coherent quantum-state manipulation of trapped atomic ions*, J.Res.Natl.Inst.Stand.Tech. **103**, 259 (1998); E. Wigner, *On the Interaction of Electrons in Metals*, Phys. Rev. **46**, 1002 (1934).
- ⁹² V. L. Berezinskii, *Destruction of long-range order in one-dimensional and two-dimensional systems possessing a continuous symmetry group*, Sov. Phys. JETP **34**, 610 (1972).
- ⁹³ J. M. Kosterlitz and D. J. Thouless, *Ordering, metastability and phase transitions in two-dimensional systems*, J. Phys. C: Solid State Physics **6**, 1181 (1973).
- ⁹⁴ R. K. Kalia and P. Vashishta, *Interfacial colloidal crystals and melting transition*, J. Phys. C **14**, L643 (1981).
- ⁹⁵ M. Boninsegni, N. Prokof'ev, and B. Svistunov, *Worm Algorithm for Continuous-Space Path Integral Monte Carlo Simulations*, Phys. Rev. Lett. **96**, 070601 (2006).
- ⁹⁶ R. Napolitano, J. Weiner, and P.S. Julienne, *Theory of optical suppression of ultracold-collision rates by polarized light*, Phys. Rev. A **55**, 1191 (1997).
- ⁹⁷ J. Weiner, V. S. Bagnato and S. Zilio, and P. S. Julienne, *Experiments and theory in cold and ultracold collisions* Rev. Mod. Phys. **71**, 1 (1999).
- ⁹⁸ S. C. Zilio, L. Marcassa, S. Muniz, R. Horowicz, V. Bagnato, R. Napolitano, J. Weiner, and P. S. Julienne, *Polarization Dependence of Optical Suppression in Photoassociative Ionization Collisions in a Sodium Magneto-optic Trap*, Phys. Rev. Lett. **76**, 2033 (1996).
- ⁹⁹ A. V. Gorshkov, P. Rabl, G. Pupillo, A. Micheli, P. Zoller, M. D. Lukin, and H. P. Büchler, *Repulsive shield between polar molecules*, arXiv:0805.0457
- ¹⁰⁰ R. Moore and N. Read, *Nonabelions in the fractional quantum hall effect*, Nucl. Phys. B **360**, 362 (1991).
- ¹⁰¹ E. Fradkin, C. Nayak, A. Tsvelik, and F. Wilczek, *A chern-simons effective field theory for the pfaffian quantum hall state*, Nucl. Phys. B **516**, 704 (1998).
- ¹⁰² N. R. Cooper, *Exact ground states of rotating bose gases close to a Feshbach resonance*, Phys. Rev. Lett. **92**, 220405 (2004).
- ¹⁰³ M. A. Levin and X. G. Wen, *String-net condensation: A physical mechanism for topological phases*, Phys. Rev. B **71**, 045110 (2005).
- ¹⁰⁴ L. Fidkowski, M. Freedman, C. Nayak, K. Walker, and Z. Wang, *From string nets to nonabelions*, arXiv:cond-mat/0610583 (2006).
- ¹⁰⁵ J. Hubbard, *Electron correlations in narrow energy bands*, Proc. R. Soc. Lond. A **276**, 238 (1963).
- ¹⁰⁶ See, e.g.: P. A. Lee, N. Nagaosa, and X.-G. Wen, *Doping a Mott insulator: physics of high-temperature superconductivity*, Rev. Mod. Phys. **78**, 17 (2006), and references therein.
- ¹⁰⁷ D. Jaksch, C. Bruder, J.I. Cirac, C.W. Gardiner, and P. Zoller, *Cold bosonic atoms in optical lattices* Phys. Rev. Lett. **81**, 3108 (1998).
- ¹⁰⁸ W. Hofstetter, J. I. Cirac, P. Zoller, E. Demler, and M. D. Lukin, *High-temperature superfluidity of fermionic atoms in optical lattices*, Phys. Rev. Lett. **89**, 220407 (2002).
- ¹⁰⁹ T. Stöferle, H. Moritz, K. Günter, M. Köhl, and T. Esslinger, *Molecules of Fermionic Atoms in an Optical Lattice*, Phys. Rev. Lett. **96**, 030401 (2006)
- ¹¹⁰ R. Jördens, N. Strohmaier, K. Günter, H. Moritz, and T. Esslinger, *Title: A Mott insulator of fermionic atoms in an optical lattice*, arXiv:0804.4009
- ¹¹¹ S. Tewari, V. W. Scarola, T. Senthil, S. D. and Sarma, *Emergence of artificial photons in an optical lattice*, Phys. Rev. Lett. **97**, 200401 (2006).
- ¹¹² F. D. M. Haldane, *Two-dimensional strongly correlated electron systems*, edited by Z. Z. Gan and Z. B. Su, Gordon and Breach (1988).
- ¹¹³ B. Douçot, M. V. Feigel'man, L. B. Ioffe, and A. S. Iosevich, *Protected qubits and Chern-Simons theories in Josephson junction arrays*, Phys. Rev. B **71**, 024505 (2005).
- ¹¹⁴ A.Yu. Kitaev, *Anyons in an exactly solved model and beyond*, Annals of Physics **321**, 2 (2006).
- ¹¹⁵ E. Dennis, A. Yu. Kitaev, A. Landahl, and J. Preskill, *Topological quantum memory*, J. Math. Phys. **43**, 4452 (2002).
- ¹¹⁶ L. M. Duan, E. Demler, and M. D. Lukin, *Controlling spin exchange interactions of ultracold atoms in optical lattices*, Phys. Rev. Lett. **91**, 090402 (2003).
- ¹¹⁷ See e.g.: M. Lewenstein, *Ultracold atomic gases in optical lattices: mimicking condensed matter physics and beyond*, A. Sanpera, V. Ahufinger, B. Damski, A. Sen De, U. Sen, Adv. Phys. **56**, 243 (2007); D. Jaksch and P. Zoller, *The cold atom Hubbard toolbox*, Ann. Phys. **315**, 52 (2005).
- ¹¹⁸ A.S. Alexandrov, *Theory of Superconductivity*, IoP Publishing, Philadelphia (2003).
- ¹¹⁹ B. Friedrich and D. Herschbach, *Alignment and Trapping of Molecules in Intense Laser Fields*, Phys. Rev. Lett. **74**, 4623 (1995).
- ¹²⁰ G. Herzberg, *Molecular spectra and molecular structure I, Spectra of diatomic molecules.*, (Van Nostrand Reinhold, New York, 1950).
- ¹²¹ J. M. Brown and A. Carrington, *Rotational Spectroscopy of Diatomic Molecules*, (Cambridge University Press, New York, 2003).
- ¹²² B. R. Judd, *Angular Momentum Theory for Diatomic Molecules*, (Academic Press, New York, 1975).
- ¹²³ See e.g. <http://physics.nist.gov/PhysRefData/MolSpec/>
- ¹²⁴ S. Coleman, *Fate of the false vacuum: Semiclassical theory*, Phys. Rev. D **15**, 2929 (1977).
- ¹²⁵ S. Kotochigova, E. Tiesinga, and P. S. Julienne, *Photoas-*

- sociative formation of ultracold polar KRB molecules*, Eur. Phys. J. D **31**, 189 (2004).
- ¹²⁶ G.D. Mahan, *Many Particle Physics*, Kluwer Academic/Plenum Publishers, New York (2000).
- ¹²⁷ This anti-adiabatic regime is hard to achieve with cold atoms, see e.g.: F. Illuminati and A. Albus, *High-Temperature Atomic Superfluidity in Lattice Bose-Fermi Mixtures*, Phys. Rev. Lett. **93**, 090406; D.-W. Wang, M.D. Lukin, and E. Demler, *Engineering superfluidity in Bose-Fermi mixtures of ultracold atoms*, Phys. Rev. A **72**, R051604 (2005).
- ¹²⁸ H. J. Carmichael, *Statistical Methods in Quantum Optics 1*, Springer-Verlag, Berlin (1999).
- ¹²⁹ M. Ortner *et al.*, in preparation.
- ¹³⁰ For single-frequency phonons in 1D, see: S. Datta, A. Das, and S. Yarlagadda, *Many-polaron effects in the Holstein model*, Phys. Rev. B **71**, 235118 (2005).
- ¹³¹ J.E. Hirsch and E. Fradkin, *Phase diagram of one-dimensional electron-phonon systems. II. The molecular-crystal model*, Phys. Rev. B **27**, 4302 (1983); P. Niyaz, R. T. Scalettar, C. Y. Fong, and G. G. Batrouni, *Phase transitions in an interacting boson model with near-neighbor repulsion*, Phys. Rev. B **50**, 362 (1994).
- ¹³² J. M. Sage, S. Sainis, T. Bergeman, and D. DeMille, *Optical production of ultracold polar molecules*, Phys. Rev. Lett. **94** 203001 (2005).
- ¹³³ M. Movre and G. Pichler, *Resonant interaction and self-broadening of alkali resonance lines I. Adiabatic potential curves*, J.Phys. B: Atom. Molec. Phys. **10**, 2631 (1977).